

Document downloaded from:

<http://hdl.handle.net/10251/165600>

This paper must be cited as:

Gisbert-Roca, F.; Lozano Picazo, P.; Pérez-Rigueiro, J.; Guinea Tortuero, GV.; Monleón Pradas, M.; Martínez-Ramos, C. (2020). Conduits based on the combination of hyaluronic acid and silk fibroin: Characterization, in vitro studies and in vivo biocompatibility. *International Journal of Biological Macromolecules*. 148:378-390.  
<https://doi.org/10.1016/j.ijbiomac.2020.01.149>



The final publication is available at

<https://doi.org/10.1016/j.ijbiomac.2020.01.149>

Copyright Elsevier

Additional Information

1  
2  
3  
4  
5 **Conduits based on the combination of hyaluronic acid and silk fibroin:**  
6 **characterization, *in vitro* studies and *in vivo* biocompatibility**  
7

8  
9 F. Gisbert Roca<sup>a</sup>, P. Lozano Picazo<sup>c,d</sup>, J. Pérez-Rigueiro<sup>b,c,d</sup>, G.V. Guinea Tortuero<sup>b,c,d</sup>,  
10 M. Monleón Pradas<sup>a,b</sup> and C. Martínez-Ramos<sup>a,\*</sup>  
11

12 a. Center for Biomaterials and Tissue Engineering, Universitat Politècnica de València, Cno. de Vera s/n, 46022, Valencia, Spain

13 b. CIBER-BBN, Biomedical Research Networking Center in Bioengineering Biomaterials and Nanomedicine, Spain

14 c. Centro de Tecnología Biomédica. Universidad Politécnica de Madrid. 28223 Pozuelo de Alarcón (Madrid), Spain

15 d. Departamento de Ciencia de Materiales. ETSI Caminos, Canales y Puertos., Universidad Politécnica de Madrid, 28040, Madrid.

16 \*Corresponding author: Cristina Martínez Ramos. Centro de Biomateriales e Ingeniería Tisular, C.P.I. Edificio 8E, Acceso F, Nivel  
17 1, Universidad Politécnica de Valencia, Camino de Vera s/n E-46022 Valencia, España. Tel.: +34963877000; fax: +34963877276.  
18 E-mail: [cris\\_mr\\_1980@hotmail.com](mailto:cris_mr_1980@hotmail.com).  
19  
20  
21

22 **Abstract**  
23

24 We address the production of structures intended as conduits made from natural  
25 biopolymers, capable of promoting the regeneration of axonal tracts. We combine  
26 hyaluronic acid (HA) and silk fibroin (SF) with the aim of improving mechanical and  
27 biological properties of HA. The results show that SF can be efficiently incorporated  
28 into the production process, obtaining conduits with tubular structure with a matrix of  
29 HA-SF blend. HA-SF has better mechanical properties than sole HA, which is a very  
30 soft hydrogel, facilitating manipulation. Culture of rat Schwann cells shows that cell  
31 adhesion and proliferation are higher than in pure HA, maybe due to the binding motifs  
32 contributed by the SF protein. This increased proliferation accelerates the formation of a  
33 tight cell layer, which covers the inner channel surface of the HA-SF tubes.  
34 Biocompatibility of the scaffolds was studied in immunocompetent mice. Both HA and  
35 HA-SF scaffolds were accepted by the host with no residual immune response at 8  
36 weeks. New collagen extracellular matrix and new blood vessels were visible and they  
37 were present earlier when SF was present. The results show that incorporation of SF  
38 enhances the mechanical properties of the materials and results in promising  
39 biocompatible conduits for tubulization strategies.  
40  
41  
42  
43  
44  
45  
46  
47  
48  
49

50 **Keywords:** biomaterials, hyaluronic acid, silk fibroin, tissue engineering, nerve  
51 guidance conduits.  
52  
53  
54  
55  
56  
57  
58  
59

## 1. Introduction

Injuries and diseases affecting the nervous system have very high incidence and prevalence, affecting millions of people around the world. New concepts and solutions are in demand for both the central nervous system (CNS) and the peripheral nervous system (PNS). In the human CNS axons do not regenerate spontaneously after damage or degeneration, causing life-long functional deficit as in the case of spinal cord injury, traumatic brain damage or cerebral infarction [1]. Failure of axonal regeneration is probably due, among other factors, to the formation of an impenetrable glial scar, composed mainly of astrocytes, that inhibits axonal growth and myelination [2]. This causes regenerative neurons to be blocked and unable to reach their synaptic target. In the PNS there is successful endogenous axon regeneration in adult humans for distances of few centimetres [1]. Here damage is followed by a degeneration of the distal segment of the nerve, known as Wallerian degeneration, while the proximal segment of the nerve suffers only minimal damage [3,4]. After the distal segment degeneration, Schwann cells and phagocytic cells such as macrophages remove myelin and axonal debris while producing cytokines that improve the axonal growth, creating a growth cone able to direct axon regrowth until reconnection with the distal target. Finally, Schwann cells myelinate the re-growing axon forming new myelin sheaths [4,5]. Nonetheless, in cases of larger damages the process of regeneration is not successful.

In order to improve over the limitations of current therapies tissue engineering approaches invoke the combination of cell supply, bioactive molecules and scaffolds based on biomaterials [6,7]. conduits typically consist in hollow tubes used to connect the two ends of a damaged nerve, guiding the axonal regeneration between both sides of the injury [8]. Their main goal is to protect the spontaneous regeneration process. Conduits must guide tissue regeneration from one end to the other of the lesion, avoiding the growth of fibrous tissue and retaining the neurotrophic factors secreted by the damaged nerve remnants [9]. Tubular scaffolds should have a porosity large enough to allow the exchange of oxygen and nutrients, and small enough to prevent the infiltration of inflammatory cells into the conduit and to minimize the outflow of cells and growth factors out of the structure; furthermore, they should possess adequate mechanical properties to allow its manipulation during surgery and be flexible and soft enough not to compress the regenerated axons [6,9].

119  
120  
121 Here we present conduits made from hyaluronic acid (HA), a natural biomaterial that  
122 is widely present in the extracellular matrix of most tissues [10]. HA is a non-branched  
123 glycosaminoglycan formed by repetitions of D-glucuronic acid and D-N-  
124 acetylglucosamine [10]. HA has an excellent biocompatibility and unique biological  
125 properties, as it regulates the immune and inflammatory response, the cell  
126 differentiation, the vascularization, the scar tissue formation and the cell adhesion to  
127 extracellular matrix (ECM) proteins [10,11]. In addition, HA modulates the behaviour  
128 of glial and immune cells [10]. A very important characteristic of HA is its high  
129 hydrophilicity, due to hydrogen bonding interactions between its chains and water  
130 [12,13]. Scaffolds made out of HA have been studied for the regeneration of the CNS,  
131 showing their biocompatibility and ability to induce neural regeneration [14–18].  
132  
133

134  
135  
136  
137  
138  
139 Tubular scaffolds made out of HA are able to induce seeded Schwann cells to form  
140 highly organized structures in vitro [19,20]. The HA tubes acted as a template in  
141 organizing the growth of the Schwann cells into cylindrical cell sheets. To improve the  
142 properties of such biohybrids (structures composed by NGCs with cells) and their  
143 biological response here we incorporate *Bombyx mori* silk fibroin (SF) in the production  
144 process of the scaffolds. SF is the term conventionally used for referring to the heavy  
145 chain protein which is the main constituent of the silk fibers of the cocoons [21]. SF is  
146 a protein with a molecular weight in excess of 300 kDa [22] that presents the specific  
147 motif of sequence –GAGAGS–. Due to its biological function, SF has robust  
148 mechanical properties and, in addition, a notable biocompatibility [23] and remarkable  
149 cell adhesion. This latter property might be favoured by the presence of arginine  
150 residues in the sequence of SF. The arginine residues might be recognized by cell  
151 membrane adhesion proteins such as integrins and would contribute to the good  
152 biological response to the material [22–25]. Besides its excellent in vitro and in vivo  
153 biocompatibility SF also shows a slow proteolytic biodegradation [23,26–28].  
154  
155  
156  
157  
158  
159  
160  
161  
162  
163  
164  
165  
166  
167  
168  
169  
170  
171  
172  
173  
174  
175  
176  
177

178  
179  
180 and SF previously studied, these are based on the physical [42], covalent [44] or  
181 enzymatic [39] cross-linking of both materials, being the SF the majority component.  
182

183 The present work aimed at combining SF and HA in a way such that the cell-  
184 templating ability of the HA tubes was preserved, while their mechanical properties and  
185 biological response were improved. Our interest thus was in combining both materials  
186 but with a majority fraction of HA. It may be noted that both HA and SF are materials  
187 currently approved by the United States Food and Drug Administration (FDA) for  
188 different uses in biomedical applications in humans, particularly in guidance of  
189 peripheral nerve regeneration. [45–48].  
190  
191  
192  
193  
194

## 195 196 **2. Materials and methods**

### 197 198 199 *2.1. SF preparation*

200  
201  
202  
203 Fibroin was extracted from *Bombyx mori* cocoons. Initially, the cocoons were  
204 degummed in an aqueous  $\text{Na}_2\text{CO}_3$  solution (0.2 w/v) and heated to 121 °C in an  
205 autoclave (Sturdy SA-252F) for 50 minutes. The degumming process solubilizes the  
206 sericin coating that covers the fibroin fibers, so that it can be removed. Fibroin was  
207 washed with distilled water for 20 minutes and the washing step was repeated three  
208 times. The fibers were allowed to dry overnight and then immersed in a 9.3 M LiBr  
209 solution and introduced in a furnace at 60 °C for 4 hours, so that a fibroin solution was  
210 obtained. After being dissolved, the silk solution was dialyzed against deionized water  
211 to remove the LiBr salt. Dialysis membranes (BioDesign Dialysis Tubing) with a  
212 MWCO of 3500 Da were used. Water was changed every 8 hours and the whole process  
213 proceeded for 48 hours. After dialysis the fibroin solution was centrifuged at 5000 rpm  
214 for 20 minutes at 21 °C to remove any debris. Finally, the fibroin was lyophilized and  
215 stored in a freezer at -20 °C.  
216  
217  
218  
219  
220  
221  
222  
223  
224

### 225 226 *2.2. HA and HA-SF films preparation*

227  
228  
229 A 5 % w/w solution of HA derived from *Streptococcus equi* (1.5-1.8 MDa, 53747,  
230 Sigma-Aldrich) in NaOH 0.2 M was elaborated by gently stirring for 24 hours under  
231 normal conditions of temperature and pressure (NCTP, 25 °C, 100 kPa). The solution  
232  
233  
234  
235  
236

237  
238  
239 was then homogenized by agitation at NCTP for 20 minutes and mixed with the divinyl  
240 sulfone cross-linker (DVS; V3700, Sigma-Aldrich) in a 9:10 DVS:HA monomeric units  
241 molar ratio. This mixture (hereinafter referred to as HA) was kept under stirring for 10  
242 seconds to achieve the correct mixing and to begin the crosslinking process.  
243  
244

245 The elaboration of biomaterials based on the combination of HA and SF is analogous  
246 to that of HA, with the exception that, after the elaboration of the HA solution, it was  
247 mixed with SF in a concentration of 3 % w/v (hereinafter referred to as HA-SF). The  
248 process was then continued by homogenization of the solution by stirring for 20 minutes  
249 and cross-linking with DVS, as it was done for HA.  
250  
251

252 Then, the material was injected by pipetting into a polytetrafluoroethylene (PTFE)  
253 mold formed by two flat faces on both sides of a U-shaped intermediate plate. After the  
254 injection of the material into the mold, it was left for 1 hour in NCTP to achieve the  
255 complete crosslinking of the material. Afterwards, it was frozen for 4 hours at -20 °C  
256 and then for 24 hours at -80 °C. Once frozen, the material was lyophilized (LyoQuest-  
257 85, Telstar Life Science) for 24 hours at 20 Pa and -80 °C. Finally, the different parts of  
258 the mold were separated to proceed to the extraction of the film.  
259  
260  
261  
262  
263  
264  
265

### 266 *2.3. HA and HA-SF conduits preparation*

267  
268  
269

270 To obtain the conduits, the biomaterials obtained as described in 2.1.2 were injected  
271 by pipetting into a PTFE mold formed by elongated channels with a square profile of  
272 2 mm per side. A polycaprolactone fiber (PCL; Polysciences) with a diameter between  
273 950 and 1050 µm was introduced into the center of each channel to form the lumen of  
274 the conduit. At both ends of the PCL fiber, a PTFE sheath was inserted with a thickness  
275 slightly greater than 2 mm. By pressing the ends of the fiber it was fixed in the center of  
276 the channel at the same approximate distance from all the walls. After the injection of  
277 the material into the mold, it was left for 10 minutes in NCTP to achieve the complete  
278 crosslinking of the material. Subsequently, it was subjected to freezing and  
279 lyophilization with the same parameters used for films. Finally, the PCL fibers were  
280 removed from the inside, forming the lumen of the conduit.  
281  
282  
283  
284  
285  
286

287 To study the effect of the dissolution of SF in a basic medium, unprocessed SF  
288 (hereinafter referred to as untreated SF) was compared with a 3 % w/v SF solution in  
289 deionized water (hereinafter referred to as water-treated SF) and with a 3 % w/v SF  
290  
291  
292  
293  
294  
295

296  
297  
298 solution in NaOH 0.2 M (hereinafter referred to as NaOH-treated SF). The solutions  
299  
300 were homogenized by stirring in NCTP for 20 minutes and then they were spilled into a  
301  
302 PTFE plate to give them a film shape. They were then frozen and lyophilized with the  
303  
304 same parameters as the other films.

#### 305 306 *2.4. Morphology characterization*

307  
308  
309 For the characterization of the surface morphology and of the geometry of axial  
310  
311 and cross-sectional cuts of conduits, a field emission scanning electron microscope  
312  
313 (FESEM; ULTRA 55, ZEISS Oxford Instruments) was used. The preparation of the  
314  
315 samples consisted primarily in a desiccation under vacuum conditions during the 24  
316  
317 hours prior to the test to avoid interferences due to evaporated water. Subsequently  
318  
319 samples were placed on a carbon tape and a carbon bridge was created between the  
320  
321 sample and the carbon tape. Finally, samples were coated with a thin layer of platinum.  
322  
323 Conduits were cut longitudinally and transversally to observe the interior of the lumen  
324  
325 and the morphology of the porosity of the walls. The voltage used was 2 kV. The study  
326  
327 was performed with three different samples (n = 3) made of HA and HA-SF.

#### 328 329 *2.5. Elemental analysis*

330  
331 The FESEM was also used to carry out an elemental analysis through an energy  
332  
333 dispersive X-ray spectroscopy (EDS) to verify the presence of SF, by studying the  
334  
335 nitrogen (N) content. Samples were prepared as above. The elemental analysis provided  
336  
337 the mass fraction ( $\omega$ ) of N, oxygen (O) and sulfur (S) in each selected area of the  
338  
339 material. The voltage used was 2 kV. The study was performed with three different  
340  
341 samples (n = 3) of films made of HA and HA-SF.

#### 342 343 *2.6. Stability against swelling and drying cycles*

344  
345 This study was carried out to evaluate the possible loss of material in cycles of  
346  
347 swelling and drying. For this purpose, both the amount of non-crosslinked mass and the  
348  
349 water uptake were studied. Disc-shaped films of 8 mm dry diameter ( $D_0$ ) of HA and  
350  
351 HA-SF were used. Samples were first vacuum desiccated for 6 hours at 50 °C. They  
352  
353  
354

355  
356  
357 were then weighed ( $m_0$ ) using a balance (AX205, Mettler-Toledo Inc., sensitivity of  
358 0.01 mg). After that, discs were swollen in deionized water for 24 hours to attain the  
359 maximum degree of swelling and the diameter was measured ( $D_1$ ). The process was  
360 then carried out a second time: samples were first air-dried for 6 hours and then dried in  
361 a desiccator for 6 hours with continuous vacuum and a temperature of 50 °C; they were  
362 then weighed ( $m$ ). Finally, discs were swollen in deionized water for 24 hours and the  
363 diameter was measured ( $D_2$ ). To study the loss of mass, the parameter  $m/m_0$  was  
364 calculated, while the water uptake was characterized through the parameter  $D_i/D_0$  for  
365 the first ( $i=1$ ) and the second ( $i=2$ ) swelling. The swelling ratio ( $Q$ ) was also calculated  
366 as  $(D_i/D_0)^3$  for the first ( $i=1$ ) and the second ( $i=2$ ) swelling. The procedure was  
367 repeated for 4 different discs ( $n = 4$ ) of each material.  
374

### 377 *2.7. Dimensional change in swelling*

378  
379  
380 To study the swelling characteristics, conduits dimensions were measured  
381 before and after the absorption of water. For this purpose, conduits made of HA and  
382 HA-SF were prepared with two different lengths: samples of approximately 4 mm in  
383 length to study the change in length and samples of approximately 1 mm in length to  
384 study changes in the lumen diameter. Samples were examined and photographed using a  
385 binocular magnifying glass (MZ APO, Leica Microsystems). Once images of dry  
386 samples were acquired, they were swollen in deionized water for 24 hours and images  
387 in swelling state were acquired. The measurement of the dimensions was performed  
388 using the ImageJ/FIJI image processing software [49]. The dimensions (length, lumen  
389 diameter) in dry and swollen conditions were calculated for 4 different samples ( $n=4$ ).  
390 The variation of the dimensions of the conduits was calculated by the ratios  $L/L_0$   
391 (length in swelling state ( $L$ ) divided by length in dry state ( $L_0$ )) and  $D/D_0$  (lumen  
392 diameter in swelling state ( $D$ ) divided by lumen diameter in dry state ( $D_0$ )).  
393  
394  
395  
396  
397  
398  
399  
400

### 401 *2.8. Density and porosity*

402  
403  
404  
405  
406 Density and porosity of samples were determined gravimetrically, using a  
407 balance (AX205, Mettler-Toledo Inc., sensitivity of 0.01 mg) equipped with a density  
408 measurement kit. First, the weight of the NGC in air ( $W_a$ ) was measured. Subsequently,  
409  
410  
411  
412  
413



414  
415  
416 the sample was immersed in n-octane (n-octane: 412236, Sigma-Aldrich) and placed  
417  
418 under vacuum for 30 minutes to replace the air inside the pores by n-octane. After  
419  
420 removing the n-octane from the lumen of the conduit with an absorbent paper, the  
421  
422 weight of the conduits was measured with n-octane in the pores ( $W_p$ ). Finally, the NGC  
423  
424 with n-octane in the pores was completely submerged in n-octane and the apparent  
425  
426 weight of the conduits immersed in n-octane ( $W_i$ ) was measured. Following  
427  
428 Archimedes, the density of the sample without considering the air inside the pores was  
429  
430 obtained applying equation (1), where  $\rho_o$  is the density of n-octane. The porosity was  
431  
432 then calculated applying equation (2). This procedure was performed for 3 samples (n =  
433  
434 3) of HA and HA-SF.

$$434 \text{ Density} = \frac{W_a}{W_a - W_i} \cdot \rho_o \quad (1)$$

$$438 \text{ Porosity} = \frac{V_{pores}}{V_{total}} = \frac{W_p - W_a}{W_p - W_i} \quad (2)$$

### 442 2.9. Thermogravimetric analysis (TGA)

445 A thermogravimetric analyzer (TGA/SDTA 851 Mettler-Toledo operated using the  
446  
447 STARexx software) was used to study the thermal degradation and composition of the  
448  
449 materials. To study the effect of the basic manufacture conditions on SF, untreated,  
450  
451 water-treated and NaOH-treated samples of SF were measured. Samples were first  
452  
453 maintained at a temperature of 30 °C for 2 minutes. Then a heating ramp was applied  
454  
455 from 30 °C to 120 °C with a heating rate of 10 °C/min. After that, a preheating stage  
456  
457 consisting of maintaining a temperature of 120 °C for 30 minutes was applied to  
458  
459 eliminate all the water content of the sample. Finally, a heating ramp was applied from  
460  
461 120 °C to 720 °C with a heating rate of 10 °C/min. The procedure was performed under  
462  
463 a positive nitrogen flow ( $N_2$ ) of 20 ml/min and was repeated for three different samples  
464  
465 (n=3) of each of the materials mentioned above. As a result, thermograms in which the  
466  
467 mass loss of the sample is represented as a function of temperature were obtained.  
468  
469 These curves were normalized dividing through the weight existing at the end point of  
470  
471 the preheating plateau.  
472

473  
474  
475 Assuming that thermal degradation proceeds in composite HA-SF samples as it  
476 would for both pure separate components, an estimate of mass loss in composites is  
477 given by equation (3), where  $\Delta m_{\text{HA}}$  and  $\Delta m_{\text{SF}}$  are the experimental curves of pure HA  
478 and SF, respectively, and  $\omega_{\text{SF}}$  is the mass fraction of SF.  
481

$$\Delta m_{\text{comp}} = \omega_{\text{SF}} \cdot \Delta m_{\text{SF}} + (1 - \omega_{\text{SF}}) \cdot \Delta m_{\text{HA}} \quad (3)$$

482  
483  
484  
485  
486  
487  
488 This equation was employed to deduce a value of  $\omega_{\text{SF}}$  from the measured curves of  
489  $\Delta m_{\text{HA}}$ ,  $\Delta m_{\text{SF}}$ ,  $\Delta m_{\text{exp}}$ . For this purpose,  $\Delta m_{\text{comp}}$  given by equation (3) was least-squares  
490 fitted to  $\Delta m_{\text{exp}}$  taking  $\omega_{\text{SF}}$  as fitting parameter.  
491  
492  
493  
494

#### 495 *2.10. Characterization of mechanical properties*

496  
497  
498 The mechanical characterization of the materials was performed by rotational  
499 rheometry (Discovery Hybrid Rheometer DHR, TA Instruments) in order to study the  
500 effect of incorporating SF on the shear modulus (G) of the material. The samples  
501 (circular films 20 mm in diameter) were studied in a state of swelling in deionized water  
502 for 24 hours.  
503  
504  
505

506 An oscillation test was performed with a frequency of 1 Hz and torque amplitudes  
507 ranging from 10 to 100  $\mu\text{N} \cdot \text{m}$  with a logarithmic sweep. Since the samples' diameter,  
508 20 mm, didn't coincide with the diameter of the rheometer plates, 25 mm, the modulus  
509 values calculated by the equipment's software were corrected to take this mismatch into  
510 account, by multiplying the software's data with the ratio of both areas.  
511  
512  
513  
514  
515

#### 516 *2.11. Schwann cell culture*

517  
518  
519 Culture of rat Schwann cells (rSCs; P10301, Innoprot) was performed on 8 mm  
520 diameter films and on NGCs made of HA and HA-SF to study the cell adhesion and  
521 proliferation.  
522  
523

524 A sanitization of the materials (films and conduits) was first carried out by  
525 immersion in 70 % ethanol (ET00021000, Scharlab) for 2 hours, in 50 % ethanol for  
526 10 minutes and in 30 % ethanol for another 10 minutes. Thereafter the ethanol residues  
527  
528  
529  
530  
531

532  
533  
534 were removed by performing 3 washes of 10 minutes with ultrapure water (Mili-Q®).  
535  
536 The preconditioning of the materials was done by immersion in culture medium  
537 (Dulbecco's modified Eagle medium with a high glucose level (4.5 g/L) (DMEM;  
538 21331020, Life Technologies) supplemented with 10 % of fetal bovine serum (FBS;  
539 10270-106/A3381E, Life Technologies) and 1 % penicillin/streptomycin (P/S;  
540 15140122, Life Technologies)) and incubation at 37 °C for 24 hours in a humidified  
541 atmosphere containing 5 % CO<sub>2</sub>.  
542  
543  
544

545 After the expansion of the rSCs in a cell culture flask, they were washed with PBS  
546 and a trypsin/EDTA solution (T/E; 25200-072, Life Technologies) was then added to  
547 break the cell-matrix and cell-cell interactions in order to remove the cells from the  
548 bottom of the culture bottle. After centrifugation at 1080 rpm for 5 minutes, the pellet  
549 was resuspended in Schwann cell culture medium (P60123, Innoprot). At this moment,  
550 the seeding with rSCs in passage 5 was performed with a seeding density of 10.000  
551 cells per film and 250.000 cells per NGC. Finally, the culture was introduced in an  
552 incubator at 37 °C with a humid atmosphere containing 5 % CO<sub>2</sub> for 1 and 5 days in the  
553 case of films and for 1, 5 and 10 days in the case of NGCs, renewing the Schwann cell  
554 culture medium every 48 hours.  
555  
556  
557  
558  
559  
560  
561  
562

### 563 *2.12. Fluorescent staining of the cytoskeleton*

564  
565

566 The morphologies of the cells were examined by fluorescently staining their F-actin  
567 cytoskeletons. Stains were performed on the cultured rSCs to carry out the labelling of  
568 specific proteins and observe the cellular arrangement. The following procedure was  
569 repeated after 1 and 5 days of culture in the case of films and after 1, 5 and 10 days in  
570 the case of conduits.  
571  
572  
573

574 First, the Schwann cell medium was removed and the materials (films and conduits)  
575 were washed with PBS. Thereafter, cells were fixed with 4 % paraformaldehyde (PFA;  
576 47608, Sigma-Aldrich) for 20 minutes at room temperature. After cell fixation, 3  
577 washes of 10 minutes with DPBS were performed to remove PFA residues. At this  
578 point, the non-specific bindings were blocked and the cell membrane was permeabilized  
579 by the use of a blocking buffer composed of DPBS with 3 % bovine serum albumin  
580 (BSA; A7906, Sigma-Aldrich) and 0.1 % Tween20 (P1379, Sigma-Aldrich) for 45  
581 minutes at room temperature. Cells were finally stained with FITC-phalloidin (B607,  
582 Life Technologies) to mark the cytoskeleton actin filaments (green colour) and with  
583  
584  
585  
586  
587  
588  
589  
590

591  
592  
593 DAPI (D9564, Sigma-Aldrich) at a 1/5000 dilution for 10 minutes to mark the cells  
594 nuclei (blue colour). The imaging was performed using a confocal microscope (LEICA  
595 TCS SP5, Leica microsystems).  
596  
597

598 From the images obtained by confocal microscopy, and thanks to staining with  
599 FITC-phalloidin, the total area occupied by the cells cytoskeleton was calculated.  
600 ImageJ/FIJI image processing software was used for this purpose [49]. Four different  
601 samples (n = 4) of HA and HA-SF films and conduits were studied.  
602  
603  
604  
605

### 606 *2.13. MTS cell proliferation assay*

607  
608

609 To evaluate the cell proliferation inside the conduits, MTS assays (CellTiter 96  
610 Aqueous One Solution Cell Proliferation Assay, Promega) were carried out on HA and  
611 HA-SF conduits (n = 3 each). When incorporated to the cells, the MTS was bio-reduced  
612 by metabolically active cells at different times of cell culture (1, 5 and 10 days) in a rate  
613 proportional to the number of live cells. After 3 hours of incubation with the reagent,  
614 the medium was removed and its absorbance was measured with a Victor Multilabel  
615 Counter 1420 spectrophotometer (Perkin-Elmer) at 490 nm.  
616  
617  
618  
619  
620  
621

### 622 *2.14. Biocompatibility of subcutaneously implanted scaffolds*

623  
624

625 All procedures were performed under the Spanish Regulations for animal  
626 experimentation (Laws 53/2013, 178/2004) with the approval of Animal Care  
627 Committee of the Polytechnic University of Madrid (Madrid, Spain) and according to  
628 the ARRIVE (Animal Research: Reporting In Vivo Experiments) guidelines. In vivo  
629 studies were conducted in adult male CD-1 mice (35-40 g body weight; 12-15 weeks  
630 old; n=5 mice for each group). All mice were bred and housed in the animal facility of  
631 the Centre for Biomedical Technology. All animals were kept at constant temperature  
632 ( $\pm 22^{\circ}\text{C}$ ) and humidity ( $\sim 52\%$ ) with free access to food and water in 12 hours light/dark  
633 cycle.  
634  
635  
636  
637  
638  
639

640 HA and HA-SF scaffolds (1.5 x 6 mm) were subcutaneously implanted at different  
641 locations in each mouse to compare the bioresponse of both scaffolds in the same  
642 animal and reduce data dispersion due to inter-animal variability. A sanitization of the  
643 materials was previously carried out by immersion in 70 % ethanol for 2 hours, in 50 %  
644 ethanol for 10 minutes and in 30 % ethanol for another 10 minutes. Afterwards the  
645  
646  
647  
648  
649

650 ethanol residues were removed by performing 4 washes of 10 minutes with ultrapure  
651 water. The preconditioning of the materials was done by immersion in PBS for 24  
652 hours.  
653  
654  
655  
656

657 Surgeries were performed under anaesthesia with 2% Isoflurane in air. The back of  
658 each mouse was shaved, and the skin was disinfected with povidone-iodine. All  
659 surgeries were made under aseptic conditions and Vaseline was administered to protect  
660 the eyes from dehydration. To implant the scaffolds, an incision of approximately 1 cm  
661 was made on the dorsal part of each mouse and the subcutaneous space was separated  
662 with scissors. The incisions were then sutured with 3-0 surgical Nylon. Buprenorphine  
663 (0.05-0.1 mg/kg) was administered as a pain reliever for 48 hours post-surgery and, if  
664 signs of pain were seen, Ibuprofen (30 mg/kg) was dispensed via oral in drinking water  
665 for 1 week. All animals were then carefully monitored for the following 3 days by  
666 animal care services. Sham-operated animals as negative controls were subjected to  
667 identical procedures, but no scaffolds were implanted in this case.  
668  
669  
670  
671  
672  
673  
674

675 At different time points after scaffolds implantation (1, 4 and 8 weeks), the mice  
676 were euthanized in 100 % CO<sub>2</sub> atmosphere (5-10 min) followed by cervical dislocation.  
677 The dorsal skin was carefully resected and immediately immersed in PBS solution. The  
678 skin sections containing the scaffolds together with the surrounding tissues were excised  
679 and fixed in 4% paraformaldehyde for 7 days. Before cutting, skin sections were  
680 cryoprotected in 30% sucrose. Samples were embedded in optimal cutting temperature  
681 compound and serial 10 µm thick sections were cut with a Microm HM550 cryostat  
682 (Thermo Scientific, Kalamazoo, USA). Cryostat sections were stained with  
683 hematoxylin-eosin (H&E) and Masson's trichrome. To examine cell infiltration,  
684 extracellular matrix deposition and neovascularisation, micrographs were captured  
685 through an Olympus BX51 microscope (Olympus DP70, Olympus America Inc. Center  
686 Valley, PA, EEUU).  
687  
688  
689  
690  
691  
692  
693  
694

### 695 *2.15. Statistical analysis*

696  
697

698 Results were expressed as mean ± standard deviation (SD). The statistical  
699 analysis of the results was performed with the software GraphPad Prism 6 using the  
700 non-parametric Mann-Whitney test based on rank comparison. Statistically significant  
701 differences are indicated by an asterisk (\*), indicating a p-value below 0.05. Four  
702 asterisks (\*\*\*\*) indicate a p-value below 0.0001.  
703  
704  
705  
706  
707  
708

709  
710  
711 **3. Results and discussion**  
712

713 *3.1. Effect of preparation procedures on material composition*  
714

715  
716 The crosslinking reaction of HA with DVS takes place in basic pH [10]. Since an  
717 aqueous solution of SF was mixed with the basic HA-DVS solution during the material  
718 preparation process, it was necessary to assess the effect of exposure of SF to the basic  
719 solution. A thermogravimetric analysis (TGA) of untreated SF, water-treated SF and  
720 NaOH-treated SF (Fig. 1A) shows slight modifications of the temperature-dependent  
721 mass loss. Prolonged exposure of SF to a basic medium causes hydrolysis of peptide  
722 bonds [50]. Therefore, when SF is added to the solution of 5 % HA in 0.2 M NaOH, it is  
723 subjected to a basic medium throughout the process and it suffers the hydrolysis of a  
724 number of peptide bonds. Chemical alteration of silk by immersion in a NaOH solution  
725 accumulates to the reduction in the molecular weight induced by the degumming  
726 process. It was found that this reduction is larger when  $\text{Na}_2\text{CO}_3$  is added to the  
727 degumming medium due to the resulting pH of the solution [51]. TGA data reflects an  
728 alteration as a difference in both curves in the range between 500 °C and 700 °C. Fig.  
729 1B shows the thermograms of untreated HA, NaOH-treated SF and of HA-SF films.  
730 The composite HA-SF materials have degradation patterns somehow intermediate, as  
731 expected. With these data, an estimate of the SF mass fraction in the composite sample  
732 can be obtained by least-square fitting the parameter in equation (3), as explained  
733 above. This gives a figure of  $\omega_{\text{SF, exp}} = 37 \pm 5$ , close enough to the theoretical  $\omega_{\text{SF, th}} =$   
734  $37.50 \pm 0.01$ , confirming efficient incorporation of SF to the HA matrix during the  
735 manufacturing process.  
736  
737  
738  
739  
740  
741  
742  
743  
744  
745  
746  
747

748 The different N content of SF and HA is reflected in the EDS data in Table 1.  
749 Theoretically, the mass fractions of N ( $\omega_{\text{N}}$ ) in HA and in HA-SF samples are 2.60 %  
750 and 6.75 %, respectively. As shown in Table 1, the experimental mass fractions of N  
751 were lower than the theoretical ones. It should be noted that the elemental analysis is  
752 performed on very small areas of material, so a non-homogeneous distribution of SF  
753 could produce this difference. In addition, elemental analysis by EDS is sensitive solely  
754 to surface composition. Table 1 shows also the ratios between  $\omega_{\text{N}}$  and the mass  
755 fractions of O and S. All these parameters were substantially higher in the HA-SF  
756 samples than in the HA samples, proving the presence of SF in the matrices.  
757  
758  
759  
760  
761  
762  
763  
764  
765  
766  
767

### 3.2. Stability against swelling and drying cycles

The loss of mass of HA and HA-SF films after prolonged immersion in water was analysed to determine the stability against solution of the SF incorporated to the HA matrix, and whether the presence of SF could alter the sol fraction of HA in the crosslinked gel. As seen on Table 1, there were no significant differences in the mass loss between HA and HA-SF films after being swollen in water. A similar sol fraction (around 30 %) obtained in both systems.

Dimensional change upon swelling was expressed by computing the ratio of measured diameters of discs after swelling ( $D$ ) and dry ( $D_0$ ). Though small, the effect of SF is to constrain swelling and dimensional change, as expected (Table 1).

	HA	HA-SF
$\omega_{N_{\text{exp}}}$ [%]	$1.0 \pm 0.1$	$3.8 \pm 0.9$
$\omega_N/\omega_0$	$0.04 \pm 0.01$	$0.20 \pm 0.01$
$\omega_N/\omega_S$	$0.18 \pm 0.03$	$1.2 \pm 0.2$
$m/m_0$	$0.72 \pm 0.01$	$0.70 \pm 0.01$
$D/D_0$ (1st swelling)	$2.0 \pm 0.1$	$1.78 \pm 0.06$
$D/D_0$ (2nd swelling)	$2.1 \pm 0.1$	$1.92 \pm 0.09$
$Q$ (1st swelling)	$8 \pm 1$	$5.7 \pm 0.6$
$Q$ (2nd swelling)	$9 \pm 2$	$7 \pm 1$

Table 1. Physicochemical properties of HA and HA-SF films. The quantities are defined in the text. Mass fraction from elemental analysis ( $\omega$ ); swelling parameters: mass ( $m/m_0$ ), diameter ( $D/D_0$ ) and swelling ( $Q$ ) ratios. Values are expressed as mean  $\pm$  SD.

### 3.3. Mechanical properties of HA-SF

827  
 828  
 829 The mechanical behaviour of HA and HA-SF discs was assessed in shear  
 830 experiments, in a rotational rheometer. Fig. 2A shows the storage modulus ( $G'$ , the real  
 831 part of the complex shear modulus) obtained as a function of the oscillatory torque.  $G'$   
 832 quantifies the recoverable energy in a cycle, and thus measures the elasticity of the  
 833 material. There is a clear increase of  $G'$  in samples containing SF, practically doubling  
 834 the  $G'$  value for all the oscillation torques. This implies that the addition of SF allows  
 835 the material to store more energy without suffering permanent deformation, indicating  
 836 that interactions between SF and HA molecules make the HA chains less pliable to  
 837 deformation, resulting in a greater stiffness of the material. There is a slight decrease in  
 838  $G'$  when the magnitude of the applied torque increases. This non-linear behaviour of the  
 839 material is indicative of strain-softening, and may be due to the rupture of SF $\cdots$ HA and  
 840 HA $\cdots$ HA intermolecular interactions with larger values of torque. The loss modulus ( $G''$ ,  
 841 the imaginary part of the complex shear modulus) is shown on Fig. 2B.  $G''$  is a measure  
 842 of the non-recoverable energy in a cycle due to different dissipative processes, and  
 843 characterizes the viscous component of the material's response. Large values of  $G''$  are  
 844 typical of soft hydrogels, and originate in internal friction due to water diffusion and  
 845 chain slippage during deformation. Presence of SF in the material results in an increase  
 846 of  $G''$ , especially for low torque amplitudes, where the increase is almost double. This is  
 847 indicative of the occurrence of new, additional frictional processes in the medium,  
 848 arising from the SF $\cdots$ HA interactions as relative slippage and as formation and diffusion  
 849 of defects. When the oscillation torque exceeds  $40 \mu\text{N} \cdot \text{m}$ , the difference decreases  
 850 considerably. The fact that this difference is sensibly higher at lower deformations may  
 851 suggest that it be related to the diffusion of water molecules in both gels, which is  
 852 altered in the presence of the protein molecules. As already commented, the stiffness of  
 853 the HA-SF material, as characterized by  $G'$ , is greater than that of HA; however, its  
 854 viscoelasticity, as characterized by the ratio  $G'/G''$ , doesn't change very much (see Table  
 855 2).

	HA		HA-SF	
	$10 \mu\text{N} \cdot \text{m}$	$100 \mu\text{N} \cdot \text{m}$	$10 \mu\text{N} \cdot \text{m}$	$100 \mu\text{N} \cdot \text{m}$
$G'/G''$	$6.8 \pm 0.7$	$6 \pm 1$	$7 \pm 2$	$7 \pm 2$



886  
887  
888 Table 2. G'/G'' ratios for HA and HA-SF at two different torque values, 10  $\mu\text{N} \cdot \text{m}$  and  
889 100  $\mu\text{N} \cdot \text{m}$ . Values are expressed as mean  $\pm$  SD.  
890  
891

### 892 893 3.4. Adhesion and proliferation of Schwann cells on HA-SF films 894

895  
896 Rat Schwann cells (rSCs) were seeded and cultured for 1 and 5 days on HA and HA-  
897 SF films in order to assess differences in adherence and proliferation. For the  
898 visualization of the cells by confocal microscopy, a staining process was performed  
899 with FITC-phalloidin 488 to visualize their cytoskeletal actin fibers (green color) and  
900 with DAPI to visualize the cell nucleus (blue color). For the day 1, Fig. 3A and 3C  
901 show representative images of both studied cases in order to appreciate the differences  
902 in the total extent of the cytoskeleton, which is indicative of the cell adhesion  
903 characteristics on the material. On HA substrates (Fig. 3A) early cell adhesion was  
904 scarce, and the cells had a marked globular morphology, in conformity with known  
905 facts [52]. This is a consequence of the highly hydrophilic nature of HA: the enormous  
906 amounts of water molecules which surround the HA chains hinder ECM protein  
907 deposition on its surface and thus difficult cell adhesion. This means that cell adhesion  
908 on the surface of HA materials must rely primarily on physical phenomena such as the  
909 surface roughness, where differential accumulation of HA molecules offers more stable  
910 anchoring sites to ECM proteins. With the material containing SF (Fig. 3C) early cell  
911 adhesion was clearly greater, with the cells exhibiting a much more developed  
912 cytoskeleton. Several studies have shown that SF has good cell adhesion properties  
913 [25,53]. Although the RGD (Arg-Gly-Asp) cell binding motif as such is not present in  
914 the aminoacid sequence of *Bombyx mori* SF, an amino acid sequence has been observed  
915 in a non-repetitive C-terminal region with a large number of basic amino acids,  
916 especially arginine, which play a key role in the cell adhesion properties of SF [25].  
917 Arginine residues can be recognized by transmembrane cell adhesion proteins such as  
918 integrins, which mediate in the interaction between cell and substrate [54,55].  
919  
920  
921  
922  
923  
924  
925  
926  
927  
928  
929  
930  
931  
932

933 In order to quantify somehow the extent of cell adhesion, the total area occupied by  
934 the cytoskeleton of the cells was measured (Fig. 3E), confirming the conclusions  
935 obtained in a qualitative way. It can be seen that early cell adhesion in HA films is very  
936 low, while addition of SF clearly enhances early cell adhesion.  
937  
938

939 The same features were analysed after 5 days of cell culture (Fig. 3B and 3D) in  
940 order to compare early with late cell adhesion characteristics. On HA films cells now  
941  
942  
943  
944

945 exhibited an elongated shape (arrows in Fig. 3B). Some cells have been able to attach to  
946 specific sites on the material surface due to mediated cell·HA interactions, but  
947 preferentially the cells entertain cell·cell bonds forming filamentary structures with the  
948 shape of a necklace. In contrast, cells cultured on films with SF (Fig. 3D) show larger  
949 fibrillary cytoskeleta spread on the material, indicative of a greater cell·surface  
950 interaction. When quantified (Fig. 3E), this conclusion is further reinforced.  
951  
952  
953  
954  
955  
956

### 957 958 *3.5. Morphology and physicochemical properties of conduits*

959  
960

961 Longitudinal (axial) and transverse cuts of conduits show the lumina of the  
962 conduits and the porous walls, Fig. 4. Both in HA and HA-SF conduits the lumen  
963 surface is always tighter and less porous than the walls, which is important to ensure  
964 that the cells seeded within the lumen are retained inside the conduit and cannot  
965 protrude across its walls. This is due to the fact that the surface of the PCL fiber used as  
966 a template of the lumen is hydrophobic; thus, in its vicinity non-swollen HA chains are  
967 predominant [19,20]. Water crystallization and subsequent lyophilization then produce a  
968 thin layer of denser HA close to the lumen. The pores observed in the conduit's wall  
969 matrix are produced by the phase-separation of water during the crystallization process.  
970 This structure ensures good diffusion of molecules across the conduit (water, oxygen,  
971 nutrients, factors), while efficiently retains the cells seeded inside the tube. The addition  
972 of SF to the HA matrix of the conduits thus didn't modify the main features of the  
973 original HA conduits. Fig. 4D' shows a detail of the internal surface of the HA-SF  
974 conduit, where elongated structures arranged on the surface (indicated with arrows)  
975 could correspond to SF fibers.  
976  
977  
978  
979  
980  
981  
982  
983  
984

985 The swelling behaviour of HA and HA-SF conduits was characterized by the  
986 change in dimensions of conduit length and lumen diameter, Table 3. There is no  
987 significant difference in dimensional change between HA and HA-SF samples. Though  
988 very small, the effect of SF seems to be to introduce some anisotropy in the conduit's  
989 swelling as compared with the HA tubes: the HA-SF tubes swell somewhat less than the  
990 HA tubes transversally to their axis, while they swell somewhat more axially. This may  
991 have to do with anisotropies of the SF fibril distribution induced during the phase  
992 separation of crystallized water, a process which is determined by the geometry of the  
993 heat transfer between gel and mold during cooling.  
994  
995  
996  
997  
998  
999  
1000  
1001  
1002  
1003

Table 3 shows the density and porosity of conduits made of HA and HA-SF. Regarding the density values, there's a slight decrease for HA-SF conduits, but it is not enough to show a statistical difference. This slight decrease may be due to the incorporation of SF, since SF has a lower density than HA [56,57]. Regarding the porosity values, the slight differences are not significant. This could be expected, since the pores are produced by the crystallization of the large amounts of water present in the samples, which are insignificantly influenced by the presence of the SF molecules.

	HA	HA-SF
$L/L_0$	$1.41 \pm 0.06$	$1.6 \pm 0.2$
$D_{\text{lumen}}/D_{\text{lumen}_0}$	$1.21 \pm 0.06$	$1.11 \pm 0.05$
Density [ $\text{g cm}^{-3}$ ]	$1.22 \pm 0.08$	$1.1 \pm 0.1$
Porosity [%]	$79 \pm 1$	$78 \pm 5$

Table 3. Physicochemical properties of HA and HA-SF conduits. Density was calculated by equation (1) and porosity by equation (2). Swelling ratios  $L/L_0$  (length) and  $D/D_0$  (diameter) are explained in the text. Values are expressed as mean  $\pm$  SD.

### 3.6. HA-SF-Schwann cells biohybrids

Schwann cells seeded within the lumen of HA tubular scaffolds create a continuous cylinder which adapts to the inner channel surface, which acts as a template for the formation of such a cell sheath [19,20]. In HA tubes this process needs 9 days, and it is the result of the interplay of cell proliferation and cell-cell contacts being preferred over cell-material contacts, due to the highly hydrophilic nature of the HA matrix. To study this process in HA-SF tubes rSCs were seeded and cultured for 1, 5 and 10 days. Staining with FITC-phalloidin and DAPI permit to visualize the cell cytoskeleton (green in Fig. 5) and nuclei (blue), respectively. A comparison of Fig. 5A and 5D shows that at day 1 there are already differences between both materials, cell density and spread being higher in the HA-SF tubes. At day 5 (Fig. 5B and 5E) considerable proliferation of SCs has occurred in both cases. However, while the

1063  
1064  
1065  
1066  
1067  
1068  
1069  
1070  
1071  
1072  
1073  
1074  
1075  
1076  
1077  
1078  
1079  
1080  
1081  
1082  
1083  
1084  
1085  
1086  
1087  
1088  
1089  
1090  
1091  
1092  
1093  
1094  
1095  
1096  
1097  
1098  
1099  
1100  
1101  
1102  
1103  
1104  
1105  
1106  
1107  
1108  
1109  
1110  
1111  
1112  
1113  
1114  
1115  
1116  
1117  
1118  
1119  
1120  
1121

number of cells inside the HA conduit is still not enough to form the rSCs sheath, in the case of the HA-SF conduit the cell population is already organized as a cell cylinder (arrows in Fig. 5E indicate how this sheath folds). This indicates that the higher cell adhesion and proliferation obtained by the incorporation of SF to the conduits allows us to obtain the rSCs sheath earlier when compared with NGCs based solely on HA. After 10 days culture the cell sheath is fully developed in both scaffolds, Fig. 5C and 5F. Previous studies showed that this kind of cell structure took 9 days to develop in HA tubular scaffolds [19,20]. We now see that the presence of SF protein in the HA matrix preserves the templating ability of the scaffold channel to induce the formation of the cell cylinder and accelerates it. Thus, while SF significantly increases cell adhesion on the channel surface due to the supply by SF of additional binding motifs, still cell-cell binding is preferred over cell-surface binding, as revealed by the easiness with which the cell cylinder gets unstuck from the scaffold (Fig. 5E and 5F). A MTS assay performed after 1, 5 and 10 days of cell culture (Fig. 6) shows that the presence of SF significantly translates into higher cell proliferation inside the conduits, explaining the earlier formation of the cell sheath in the HA-SF conduits.

### 3.7. *Biocompatibility of subcutaneously implanted biomaterials*

During the study there were no cases of pain, inflammation or infection caused by the implantation of scaffolds. The skin sections containing the scaffolds were photographed at 1, 4 and 8 weeks after their implantation (Fig. 7). As can be seen in Fig. 7, the scaffolds are surrounded by healthy tissue since the first week. The presence of blood vessels near to or in direct contact with the scaffolds is also always visible (white arrows in Fig. 7).

Biocompatibility of subcutaneously implanted biomaterials was assessed by H&E and Masson's trichrome staining of fixed scaffolds after its implantation for 1, 4 and 8 weeks (Fig. 8 for HA scaffolds and Fig. 9 for HA-SF scaffolds). An overall view of a representative longitudinal section of each scaffold is shown in first place (A, E and I for H&E staining; C, G and K for Masson's trichrome staining), and a magnified view of the perimeter of each biomaterial is shown in second place (B, F and J for H&E staining; D, H and L for Masson's trichrome staining), at each post-implantation time point.

1122  
1123  
1124 One week after the scaffold implantation, a moderate immune response can be  
1125 observed for both HA (Fig. 8 A-D) and HA-SF (Fig. 9 A-D) scaffolds. In both cases a  
1126 fibrous capsule surrounding the scaffold is clearly visible, which is a typical reaction  
1127 after the implantation of a biomaterial. There is also a dense population of granulocytes  
1128 surrounding the scaffolds. Notably, some collagen structures and some cross sections of  
1129 blood vessels and capillaries are present, although small and isolated.  
1130  
1131

1132  
1133  
1134 After 4 weeks, a reduction of the immune response can be observed, corresponding  
1135 to a mild foreign body reaction for both HA (Fig. 8 E-H) and HA-SF (Fig. 9 E-H)  
1136 scaffolds. The population of granulocytes has been reduced and it has infiltrated inside  
1137 the scaffold. Now, a greater presence of macrophages is observable, which indicates  
1138 that the bioresorption process of the scaffold has begun. Remarkably, there is an  
1139 increase of the number and extension of collagen structures, indicating that new  
1140 extracellular matrix is being deposited. In addition, more cross sections of blood vessels  
1141 and capillaries and more red blood cells are observable around and inside the scaffold. It  
1142 seems that this process of collagen deposition and vascularization inside the scaffold is  
1143 accelerated when SF is present, since more collagen structures and more blood vessels  
1144 can be observed inside the scaffold.  
1145  
1146  
1147  
1148  
1149  
1150

1151 Finally, after 8 weeks, the immune response has been drastically reduced, so both  
1152 HA (Fig. 8 I-L) and HA-SF (Fig. 9 I-L) scaffolds have been completely resorbed. The  
1153 fibrous capsule has disappeared and the population of granulocytes and macrophages at  
1154 the scaffold site has almost disappeared, with the epidermis tissue surrounding the  
1155 scaffold appearing normal. There is a clear increase of the deposition of collagen  
1156 structures around and inside the cavities of the scaffolds, compared with week 4, and  
1157 individual collagen fibres are clearly visible within the collagen matrix (Fig. 10). This  
1158 increased presence of collagen structures is associated to the presence of active  
1159 fibroblasts (spindle shaped cells in Fig. 10 B and Fig. 10 D for HA and HA-SF  
1160 scaffolds, respectively), that can be observed infiltrating into the scaffold from the  
1161 surrounding epidermis. Regarding the vascularization process, it is quite similar to the  
1162 one observed after 4 weeks. Multiple cross sections of blood vessels and capillaries are  
1163 observed around and inside the scaffold, as well as populations of isolated blood cells  
1164 (Fig. 10). At this time there is not a notably difference between HA and HA-SF  
1165 scaffolds regarding the collagen deposition and the vascularization.  
1166  
1167  
1168  
1169  
1170  
1171  
1172  
1173  
1174  
1175  
1176  
1177  
1178  
1179  
1180

1181  
1182  
1183 These results suggest that both HA and HA-SF scaffolds are biointegrated by the  
1184 host after 8 weeks of implantation and that, furthermore, the processes of extracellular  
1185 matrix deposition and angiogenesis are accelerated when SF is present.  
1186  
1187  
1188

## 1189 **Conclusions**

1190  
1191 Silk fibroin protein can be efficiently incorporated into the manufacturing  
1192 process of HA-based tubular scaffolds intended as nerve conduits. The developed  
1193 materials are stable over time after swelling and drying cycles. SF supplies cell-binding  
1194 sequences which lead to higher Schwann cell adhesion and proliferation in the HA-SF  
1195 materials when compared with the HA ones. While most physicochemical properties  
1196 (density, porosity and swelling degree) of both materials are indistinguishable,  
1197 manipulability and mechanical shear modulus are improved by the presence of SF. The  
1198 HA-SF tubular scaffolds can act as templates of Schwann-cell macrocylinders, as had  
1199 the HA scaffolds, but the process is significantly accelerated in HA-SF scaffolds. The  
1200 biocompatibility of both HA and HA-SF scaffolds has been proven, and both  
1201 biomaterials were accepted by the host after 8 weeks of implantation. This finding is of  
1202 importance when thinking of the HA-SF-Schwann cells constructs as transplantable  
1203 biohybrids, since it considerably shortens the in vitro and in vivo strategies, where  
1204 tubulisation techniques are required for regeneration.  
1205  
1206  
1207  
1208  
1209  
1210  
1211  
1212  
1213

## 1214 **Conflicts of interest**

1215  
1216 There are no conflicts to declare.  
1217  
1218  
1219

## 1220 **Acknowledgements**

1221  
1222 The authors acknowledge financing from the Spanish Ministry of Economy and  
1223 Competitiveness through grants RTI2018-095872-B-C22/ERDF, DPI2015-72863-EXP,  
1224 MAT2016-79832-R, MAT2016-76847-R and, and community of Madrid through grant  
1225 Neurocentro-B2017/BMD-3760. FGR acknowledges scholarship FPU16/01833 of the  
1226 Spanish Ministry of Education, Culture and Sports. We thank the Electron Microscopy  
1227 Service at the UPV, where the FESEM images were obtained.  
1228  
1229  
1230  
1231  
1232

## 1233 **References**

1234  
1235 [1] E. a Huebner, S.M. Strittmatter, Axon Regeneration in the Peripheral and Central  
1236  
1237  
1238  
1239

- 1240  
1241  
1242  
1243  
1244  
1245  
1246  
1247  
1248  
1249  
1250  
1251  
1252  
1253  
1254  
1255  
1256  
1257  
1258  
1259  
1260  
1261  
1262  
1263  
1264  
1265  
1266  
1267  
1268  
1269  
1270  
1271  
1272  
1273  
1274  
1275  
1276  
1277  
1278  
1279  
1280  
1281  
1282  
1283  
1284  
1285  
1286  
1287  
1288  
1289  
1290  
1291  
1292  
1293  
1294  
1295  
1296  
1297  
1298
- Nervous Systems, *Results Probl. Cell Differ. Author Manusc.* 48 (2009) 339–351. doi:10.1007/400.
- [2] J.W. Fawcett, R.A. Asher, The glial scar and central nervous system repair, *Brain Res. Bull.* 49 (1999) 377–391. doi:10.1016/S0361-9230(99)00072-6.
- [3] A.H. Koeppen, Wallerian degeneration: History and clinical significance, *J. Neurol. Sci.* 220 (2004) 115–117. doi:10.1016/j.jns.2004.03.008.
- [4] S. Hall, The response to injury in the peripheral nervous system., *J. Bone Jt. Surg.* 87 (2005) 1309–19. doi:10.1302/0301-620X.87B10.16700.
- [5] P. Dubový, I. Klusáková, I. Hradilová Svíženská, Inflammatory profiling of Schwann cells in contact with growing axons distal to nerve injury, *Biomed Res. Int.* 2014 (2014). doi:10.1155/2014/691041.
- [6] K.S. Houschyar, A. Momeni, M.N. Pyles, J.Y. Cha, Z.N. Maan, D. Duscher, O.S. Jew, F. Siemers, J. van Schoonhoven, K.S. Houschyar, A. Momeni, M.N. Pyles, J.Y. Cha, Z.N. Maan, D. Duscher, O.S. Jew, F. Siemers, J. van Schoonhoven, The Role of Current Techniques and Concepts in Peripheral Nerve Repair, *Plast. Surg. Int.* 2016 (2016) 1–8. doi:10.1155/2016/4175293.
- [7] L. Tian, M.P. Prabhakaran, S. Ramakrishna, Strategies for regeneration of components of nervous system: scaffolds, cells and biomolecules., *Regen. Biomater.* 2 (2015) 31–45. doi:10.1093/rb/rbu017.
- [8] A. Muheremu, Q. Ao, Past , Present , and Future of Nerve Conduits in the Treatment of Peripheral Nerve Injury, 2015 (2015). doi:10.1155/2015/237507.
- [9] S. Kehoe, X.F. Zhang, D. Boyd, FDA approved guidance conduits and wraps for peripheral nerve injury: A review of materials and efficacy, *Injury.* 43 (2012) 553–572. doi:10.1016/j.injury.2010.12.030.
- [10] H.G. Garg, C.A. Hales, *Chemistry and biology of hyaluronan*, Elsevier, 2004. [https://books.google.es/books?hl=es&lr=&id=WCjv3-\\_q2ggC&oi=fnd&pg=PP1&dq=chemistry+and+biology+of+hyaluronan&ots=FSm4Y8GDCu&sig=QdBL61rlFZbNjhWMvoX7xVZX6AU#v=onepage&q=chemistry and biology of hyaluronan&f=false](https://books.google.es/books?hl=es&lr=&id=WCjv3-_q2ggC&oi=fnd&pg=PP1&dq=chemistry+and+biology+of+hyaluronan&ots=FSm4Y8GDCu&sig=QdBL61rlFZbNjhWMvoX7xVZX6AU#v=onepage&q=chemistry+and+biology+of+hyaluronan&f=false) (accessed February 4, 2018).
- [11] M.N. Collins, C. Birkinshaw, Hyaluronic acid based scaffolds for tissue engineering - A review, *Carbohydr. Polym.* 92 (2013) 1262–1279. doi:10.1016/j.carbpol.2012.10.028.
- [12] J.E. Scott, Secondary structures in hyaluronan solutions: chemical and biological implications., *Ciba Found. Symp.* 143 (1989) 6–15; discussion 15-20, 281–5.

- 1299  
1300  
1301 <http://www.ncbi.nlm.nih.gov/pubmed/2680349> (accessed June 4, 2017).  
1302
- [13] M.K. Cowman, S. Matsuoka, Experimental approaches to hyaluronan structure,  
1303 *Carbohydr. Res.* 340 (2005) 791–809. doi:10.1016/j.carres.2005.01.022.  
1304  
1305
- [14] Y. Liang, P. Walczak, J.W.M. Bulte, The survival of engrafted neural stem cells  
1306 within hyaluronic acid hydrogels, *Biomaterials.* 34 (2013) 5521–5529.  
1307 doi:10.1016/j.biomaterials.2013.03.095.  
1308  
1309
- [15] T.-W. Wang, M. Spector, Development of hyaluronic acid-based scaffolds for  
1310 brain tissue engineering., *Acta Biomater.* 5 (2009) 2371–84.  
1311 doi:10.1016/j.actbio.2009.03.033.  
1312  
1313
- [16] J. Ma, W.-M. Tian, S.-P. Hou, Q.-Y. Xu, M. Spector, F.-Z. Cui, An experimental  
1314 test of stroke recovery by implanting a hyaluronic acid hydrogel carrying a Nogo  
1315 receptor antibody in a rat model., *Biomed. Mater.* 2 (2007) 233–40.  
1316 doi:10.1088/1748-6041/2/4/005.  
1317  
1318
- [17] W.M. Tian, S.P. Hou, J. Ma, C.L. Zhang, Q.Y. Xu, I.S. Lee, H.D. Li, M. Spector,  
1319 F.Z. Cui, Hyaluronic acid-poly-D-lysine-based three-dimensional hydrogel for  
1320 traumatic brain injury., *Tissue Eng.* 11 (2005) 513–25.  
1321 doi:10.1089/ten.2005.11.513.  
1322  
1323
- [18] M. Pérez-Garnes, J.A. Barcia, U. Gómez-Pinedo, M. Monleón Pradas, A. Vallés-  
1324 Lluch, Materials for Central Nervous System Tissue Engineering, in: *Cells*  
1325 *Biomater. Regen. Med.*, InTech, 2014. doi:10.5772/59339.  
1326  
1327
- [19] G. Vilariño-Feltrer, C. Martínez-Ramos, A. Monleón-De-La-Fuente, A. Vallés-  
1328 Lluch, D. Moratal, J.A. Barcia Albacar, M. Monleón Pradas, Schwann-cell  
1329 cylinders grown inside hyaluronic-acid tubular scaffolds with gradient porosity,  
1330 *Acta Biomater.* 30 (2016) 199–211. doi:10.1016/j.actbio.2015.10.040.  
1331  
1332
- [20] I. Ortuno-Lizarán, G. Vilarino-Feltrer, C. Martinez-Ramos, M.M. Pradas, A.  
1333 Vallés-Lluch, Influence of synthesis parameters on hyaluronic acid hydrogels  
1334 intended as nerve conduits, *Biofabrication.* 8 (2016). doi:10.1088/1758-  
1335 5090/8/4/045011.  
1336  
1337
- [21] R. J. Lancashire, *Chemistry of Garments: Animal Fibres*, Dep. Chem. Univ. West  
1338 Indies. (2011).  
1339 [http://wwwchem.uwimona.edu.jm/courses/CHEM2402/Textiles/Animal\\_Fibres.html](http://wwwchem.uwimona.edu.jm/courses/CHEM2402/Textiles/Animal_Fibres.html)  
1340 (accessed June 3, 2017).  
1341  
1342
- [22] Q. Xia, Z. Zhou, C. Lu, D. Cheng, F. Dai, B. Li, P. Zhao, X. Zha, T. Cheng, C.  
1343 Chai, G. Pan, J. Xu, C. Liu, Y. Lin, J. Qian, Y. Hou, Z. Wu, G. Li, M. Pan, C. Li,  
1344  
1345  
1346  
1347  
1348  
1349  
1350  
1351  
1352  
1353  
1354  
1355  
1356  
1357



1358  
1359  
1360 Y. Shen, X. Lan, L. Yuan, T. Li, H. Xu, G. Yang, Y. Wan, Y. Zhu, M. Yu, W.  
1361 Shen, D. Wu, Z. Xiang, J. Yu, J. Wang, R. Li, J. Shi, H. Li, G. Li, J. Su, X.  
1362 Wang, G. Li, Z. Zhang, Q. Wu, J. Li, Q. Zhang, N. Wei, J. Xu, H. Sun, L. Dong,  
1363 D. Liu, S. Zhao, X. Zhao, Q. Meng, F. Lan, X. Huang, Y. Li, L. Fang, C. Li, D.  
1364 Li, Y. Sun, Z. Zhang, Z. Yang, Y. Huang, Y. Xi, Q. Qi, D. He, H. Huang, X.  
1365 Zhang, Z. Wang, W. Li, Y. Cao, Y. Yu, H. Yu, J. Li, J. Ye, H. Chen, Y. Zhou, B.  
1366 Liu, J. Wang, J. Ye, H. Ji, S. Li, P. Ni, J. Zhang, Y. Zhang, H. Zheng, B. Mao,  
1367 W. Wang, C. Ye, S. Li, J. Wang, G.K.S. Wong, H. Yang, A draft sequence for  
1368 the genome of the domesticated silkworm (*Bombyx mori*), *Science* (80-. ). 306  
1369 (2004) 1937–1940. doi:10.1126/science.1102210.

- 1370  
1371  
1372 [23] C. Vepari, D.L. Kaplan, Silk as a biomaterial, *Prog. Polym. Sci.* 32 (2007) 991–  
1373 1007. doi:10.1016/j.progpolymsci.2007.05.013.  
1374  
1375 [24] A.R. Murphy, D.L. Kaplan, Biomedical applications of chemically-modified silk  
1376 fibroin, *J. Mater. Chem.* 19 (2009) 6443. doi:10.1039/b905802h.  
1377  
1378 [25] N. Minoura, S.I. Aiba, M. Higuchi, Y. Gotoh, M. Tsukada, Y. Imai, Attachment  
1379 and growth of fibroblast cells on silk fibroin, *208* (1995) 511–516.  
1380 doi:10.1006/bbrc.1995.1368.  
1381  
1382 [26] S. Sofia, M.B. McCarthy, G. Gronowicz, D.L. Kaplan, Functionalized silk-based  
1383 biomaterials for bone formation., *J. Biomed. Mater. Res.* 54 (2001) 139–48.  
1384 <http://www.ncbi.nlm.nih.gov/pubmed/11077413> (accessed June 30, 2017).  
1385  
1386 [27] G.H. Altman, F. Diaz, C. Jakuba, T. Calabro, R.L. Horan, J. Chen, H. Lu, J.  
1387 Richmond, D.L. Kaplan, Silk-based biomaterials., *Biomaterials.* 24 (2003) 401–  
1388 16. <http://www.ncbi.nlm.nih.gov/pubmed/12423595> (accessed June 30, 2017).  
1389  
1390 [28] R.L. Horan, K. Antle, A.L. Collette, Y. Wang, J. Huang, J.E. Moreau, V.  
1391 Volloch, D.L. Kaplan, G.H. Altman, In vitro degradation of silk fibroin.,  
1392 *Biomaterials.* 26 (2005) 3385–93. doi:10.1016/j.biomaterials.2004.09.020.  
1393  
1394 [29] N.H. Chi, M.C. Yang, T.W. Chung, N.K. Chou, S.S. Wang, Cardiac repair using  
1395 chitosan-hyaluronan/silk fibroin patches in a rat heart model with myocardial  
1396 infarction, *Carbohydr Polym.* 92 (2013) 591–597.  
1397 doi:10.1016/j.carbpol.2012.09.012.  
1398  
1399 [30] N.H. Chi, M.C. Yang, T.W. Chung, J.Y. Chen, N.K. Chou, S.S. Wang, Cardiac  
1400 repair achieved by bone marrow mesenchymal stem cells/silk fibroin/hyaluronic  
1401 acid patches in a rat of myocardial infarction model, *Biomaterials.* 33 (2012)  
1402 5541–5551. doi:10.1016/j.biomaterials.2012.04.030.  
1403  
1404  
1405  
1406  
1407  
1408  
1409  
1410  
1411  
1412  
1413  
1414  
1415  
1416

- 1417  
1418  
1419  
1420  
1421  
1422  
1423  
1424  
1425  
1426  
1427  
1428  
1429  
1430  
1431  
1432  
1433  
1434  
1435  
1436  
1437  
1438  
1439  
1440  
1441  
1442  
1443  
1444  
1445  
1446  
1447  
1448  
1449  
1450  
1451  
1452  
1453  
1454  
1455  
1456  
1457  
1458  
1459  
1460  
1461  
1462  
1463  
1464  
1465  
1466  
1467  
1468  
1469  
1470  
1471  
1472  
1473  
1474  
1475
- [31] M.C. Yang, N.H. Chi, N.K. Chou, Y.Y. Huang, T.W. Chung, Y.L. Chang, H.C. Liu, M.J. Shieh, S.S. Wang, The influence of rat mesenchymal stem cell CD44 surface markers on cell growth, fibronectin expression, and cardiomyogenic differentiation on silk fibroin - Hyaluronic acid cardiac patches, *Biomaterials*. 31 (2010) 854–862. doi:10.1016/j.biomaterials.2009.09.096.
- [32] J. Zhou, B. Zhang, X. Liu, L. Shi, J. Zhu, D. Wei, J. Zhong, G. Sun, D. He, Facile method to prepare silk fibroin/hyaluronic acid films for vascular endothelial growth factor release, *Carbohydr Polym*. 143 (2016) 301–309. doi:10.1016/j.carbpol.2016.01.023.
- [33] S. Yan, M. Li, Q. Zhang, J. Wang, Blend films based on silk fibroin/hyaluronic acid, *Fibers Polym*. 14 (2013) 188–194. doi:10.1007/s12221-013-0188-2.
- [34] C. Foss, E. Merzari, C. Migliaresi, A. Motta, Silk fibroin/hyaluronic acid 3D matrices for cartilage tissue engineering, *Biomacromolecules*. 14 (2013) 38–47. doi:10.1021/bm301174x.
- [35] J. Jaipaw, P. Wangkulangkul, J. Meesane, P. Raungrut, P. Puttawibul, Mimicked cartilage scaffolds of silk fibroin/hyaluronic acid with stem cells for osteoarthritis surgery: Morphological, mechanical, and physical clues, *Mater Sci Eng C Mater Biol Appl*. 64 (2016) 173–182. doi:10.1016/j.msec.2016.03.063.
- [36] Z. Fan, F. Zhang, T. Liu, B.Q. Zuo, Effect of hyaluronan molecular weight on structure and biocompatibility of silk fibroin/hyaluronan scaffolds, *Int J Biol Macromol*. 65 (2014) 516–523. doi:10.1016/j.ijbiomac.2014.01.058.
- [37] T.W. Chung, Y.L. Chang, Silk fibroin/chitosan-hyaluronic acid versus silk fibroin scaffolds for tissue engineering: promoting cell proliferations in vitro, *J Mater Sci Mater Med*. 21 (2010) 1343–1351. doi:10.1007/s10856-009-3876-0.
- [38] M. Garcia-Fuentes, A.J. Meinel, M. Hilbe, L. Meinel, H.P. Merkle, Silk fibroin/hyaluronan scaffolds for human mesenchymal stem cell culture in tissue engineering, *Biomaterials*. 30 (2009) 5068–5076. doi:10.1016/j.biomaterials.2009.06.008.
- [39] N.R. Raia, B.P. Partlow, M. McGill, E.P. Kimmerling, C.E. Ghezzi, D.L. Kaplan, Enzymatically crosslinked silk-hyaluronic acid hydrogels, *Biomaterials*. 131 (2017) 58–67. doi:10.1016/j.biomaterials.2017.03.046.
- [40] S. Yan, Q. Zhang, J. Wang, Y. Liu, S. Lu, M. Li, D.L. Kaplan, Silk fibroin/chondroitin sulfate/hyaluronic acid ternary scaffolds for dermal tissue reconstruction, *Acta Biomater*. 9 (2013) 6771–6782.

- 1476  
1477  
1478  
1479  
1480  
1481  
1482  
1483  
1484  
1485  
1486  
1487  
1488  
1489  
1490  
1491  
1492  
1493  
1494  
1495  
1496  
1497  
1498  
1499  
1500  
1501  
1502  
1503  
1504  
1505  
1506  
1507  
1508  
1509  
1510  
1511  
1512  
1513  
1514  
1515  
1516  
1517  
1518  
1519  
1520  
1521  
1522  
1523  
1524  
1525  
1526  
1527  
1528  
1529  
1530  
1531  
1532  
1533  
1534
- doi:10.1016/j.actbio.2013.02.016.
- [41] M. Garcia-Fuentes, E. Giger, L. Meinel, H.P. Merkle, The effect of hyaluronic acid on silk fibroin conformation, *Biomaterials*. 29 (2008) 633–642. doi:10.1016/j.biomaterials.2007.10.024.
- [42] X. Hu, Q. Lu, L. Sun, P. Cebe, X. Wang, X. Zhang, D.L. Kaplan, Biomaterials from Ultrasonication-Induced Silk Fibroin - Hyaluronic Acid Hydrogels, *Biomacromolecules*. 11 (2010) 3178–3188. doi:10.1021/bm1010504.
- [43] Y.J. Ren, Z.Y. Zhou, B.F. Liu, Q.Y. Xu, F.Z. Cui, Preparation and characterization of fibroin/hyaluronic acid composite scaffold, *Int J Biol Macromol*. 44 (2009) 372–378. doi:10.1016/j.ijbiomac.2009.02.004.
- [44] E. Pavlovic, M.A. Serban, X. Yu, N.J. Manesis, Cross-linked silk-hyaluronic acid compositions, US 2014/0315828A1, 2014. <https://patents.google.com/patent/US20140315828A1/en> (accessed July 22, 2017).
- [45] F.S. Brandt, A. Cazzaniga, Hyaluronic acid gel fillers in the management of facial aging, *Clin. Interv. Aging*. 3 (2008) 153–159.
- [46] S.-F. Sun, Y.-J. Chou, C.-W. Hsu, W.-L. Chen, Hyaluronic acid as a treatment for ankle osteoarthritis., *Curr. Rev. Musculoskelet. Med*. 2 (2009) 78–82. doi:10.1007/s12178-009-9048-5.
- [47] T. Yucel, M.L. Lovett, D.L. Kaplan, Silk-based biomaterials for sustained drug delivery, *J. Control. Release*. 190 (2014) 381–397. doi:10.1016/j.jconrel.2014.05.059.
- [48] C.J. Bettinger, K.M. Cyr, A. Matsumoto, R. Langer, J.T. Borenstein, D.L. Kaplan, Silk fibroin microfluidic devices, *Adv. Mater.* 19 (2007) 2847–2850. doi:10.1002/adma.200602487.Silk.
- [49] J. Schindelin, I. Arganda-Carreras, E. Frise, V. Kaynig, M. Longair, T. Pietzsch, S. Preibisch, C. Rueden, S. Saalfeld, B. Schmid, J.-Y. Tinevez, D.J. White, V. Hartenstein, K. Eliceiri, P. Tomancak, A. Cardona, Fiji: an open-source platform for biological-image analysis, *Nat. Methods*. 9 (2012) 676–682. doi:10.1038/nmeth.2019.
- [50] P. Taddei, E. Pavoni, M. Tsukada, Stability toward alkaline hydrolysis of B. mori silk fibroin grafted with methacrylamide, *J. Raman Spectrosc.* 47 (2016) 731–739. doi:10.1002/jrs.4892.
- [51] G.B. Perea, C. Solanas, N. Marí-Buyé, R. Madurga, F. Agulló-Rueda, A.

- 1535  
1536  
1537 Muinelo, C. Riekkel, M. Burghammer, I. Jorge, J. Vázquez, G.R. Plaza, A.L.  
1538  
1539 Torres, F. Del Pozo, G. V. Guinea, M. Elices, J.L. Cenis, J. Pérez-Rigueiro, The  
1540 apparent variability of silkworm (*Bombyx mori*) silk and its relationship with  
1541 degumming, *Eur. Polym. J.* 78 (2016) 129–140.  
1542 doi:10.1016/j.eurpolymj.2016.03.012.  
1543  
1544  
1545 [52] M. Hu, E.E. Sabelman, C. Tsai, J. Tan, V.R. Hentz, Improvement of Schwann  
1546 Cell Attachment and Proliferation on Modified Hyaluronic Acid Strands by  
1547 Polylysine, *Tissue Eng.* 6 (2000) 585–593. doi:10.1089/10763270050199532.  
1548  
1549  
1550 [53] Y. Jo, H. Kweon, K. Lee, S. Nam, H. Lee, J. Yeo, The Promotion of Cell  
1551 Attachment and Proliferation on Silk Fibroin, 54 (2011) 166–170.  
1552  
1553 [54] G.A. Monteiro, A. V Fernandes, H.G. Sundararaghavan, D.I. Shreiber, Positively  
1554 and Negatively Modulating Cell Adhesion to Type I Collagen Via Peptide  
1555 Grafting, *Tissue Eng. Part A.* 17 (2011) 1663–1673.  
1556 doi:10.1089/ten.tea.2008.0346.  
1557  
1558  
1559 [55] C. Calcagno, M.E. Lobatto, P.M. Robson, A. Millon, Mapping structural  
1560 landmarks, ligand binding sites and missense mutations to the collagen IV  
1561 heterotrimers predicts major functional domains, novel interactions and variation  
1562 in phenotypes in inherited diseases affecting basement membranes, *Hum Mutat.*  
1563 28 (2016) 1304–1314. doi:10.1002/nbm.3369.Three.  
1564  
1565  
1566 [56] A.U. Ude, R.A. Eshkoo, R. Zulkifili, A.K. Ariffin, A.W. Dzuraidah, C.H.  
1567 Azhari, *Bombyx mori* silk fibre and its composite: A review of contemporary  
1568 developments, *Mater. Des.* 57 (2014) 298–305.  
1569 doi:10.1016/j.matdes.2013.12.052.  
1570  
1571  
1572 [57] E.D.T. Atkins, C.F. Phelps, J.K. Sheehan, The conformation of the  
1573 mucopolysaccharides. Hyaluronates, *Biochem. J.* 128 (1972) 1255–1263.  
1574 doi:10.1042/bj1281255.  
1575  
1576  
1577  
1578  
1579  
1580  
1581  
1582  
1583  
1584  
1585  
1586  
1587  
1588  
1589  
1590  
1591  
1592  
1593

**Fig. 1.** A: Experimental thermograms of NaOH-treated SF (dotted line), water-treated (solid line) and untreated SF (dashed line). Values are expressed as mean  $\pm$  SD. The thermograms show that SF exposed to a basic medium suffers a chemical alteration. B: Experimental thermograms of HA (solid line), HA-SF (dashed line) and NaOH-treated SF (dotted line). Values are expressed as mean  $\pm$  SD. In the temperature range between 220 °C and 370 °C there is an intermediate behavior of the HA-SF thermogram, indicating the presence of SF. The theoretical and the experimental mass fraction of SF in the HA-SF material is also indicated.

**Fig. 2.** Storage modulus (A) and loss modulus (B) as a function of the oscillation torque for HA (circles) and HA-SF (squares). Values are expressed as mean  $\pm$  SD. Presence of SF increases both the storage and the loss moduli.

**Fig. 3.** A-D: Confocal microscopy images corresponding to rSCs cultured on HA for 1 (A) and 5 days (B) and on HA-SF for 1 (C) and 5 days (D). The cytoskeleton is shown in green and the nuclei are shown in blue. Scale bar = 30  $\mu$ m. E: Total area of rSCs cytoskeleta after 1 and 5 days of culture on HA and HA-SF. Cells cultured on HA-SF films presented a larger cytoskeleton area when compared to HA films, indicating a greater cell adhesion thanks to the presence of SF.

**Fig. 4.** FESEM images of axial cuts and cross sections of HA (A, B and B') and HA-SF (C, D and D') conduits. B' and D' show a detail of the internal surface of the conduit. Scale bar = 500  $\mu$ m (A, B, C and D) and 100  $\mu$ m (B' and D'). Matrix porosity is produced by the lyophilization process. The inner channel surface is less porous, due to the hydrophobic nature of the channel template. Arrows in D' indicate the presence of elongated structures on the surface of HA-SF conduits that may correspond to SF fibers.

**Fig. 5.** Confocal microscopy images corresponding to rSCs cultured inside HA tubes for 1 (A), 5 (B) and 10 days (C), and inside HA-SF tubes for 1 (D), 5 (E) and 10 days (F). The cytoskeleton is shown in green and the nuclei are shown in blue. Scale bars = 100  $\mu$ m. The presence of SF seems to accelerate the formation of the cell sheath, which is completely developed in the HA-SF conduits at day 5 (arrows in E showing a fold of this structure), while it took 10 days to fully develop in HA tubes (arrows in C).

**Fig. 6.** MTS proliferation assays on rSCs cultures inside HA and HA-SF conduits at different culture times (1, 5 and 10 days). The presence of SF increases cell proliferation, explaining the earlier formation of the cell sheath in the HA-SF conduits.

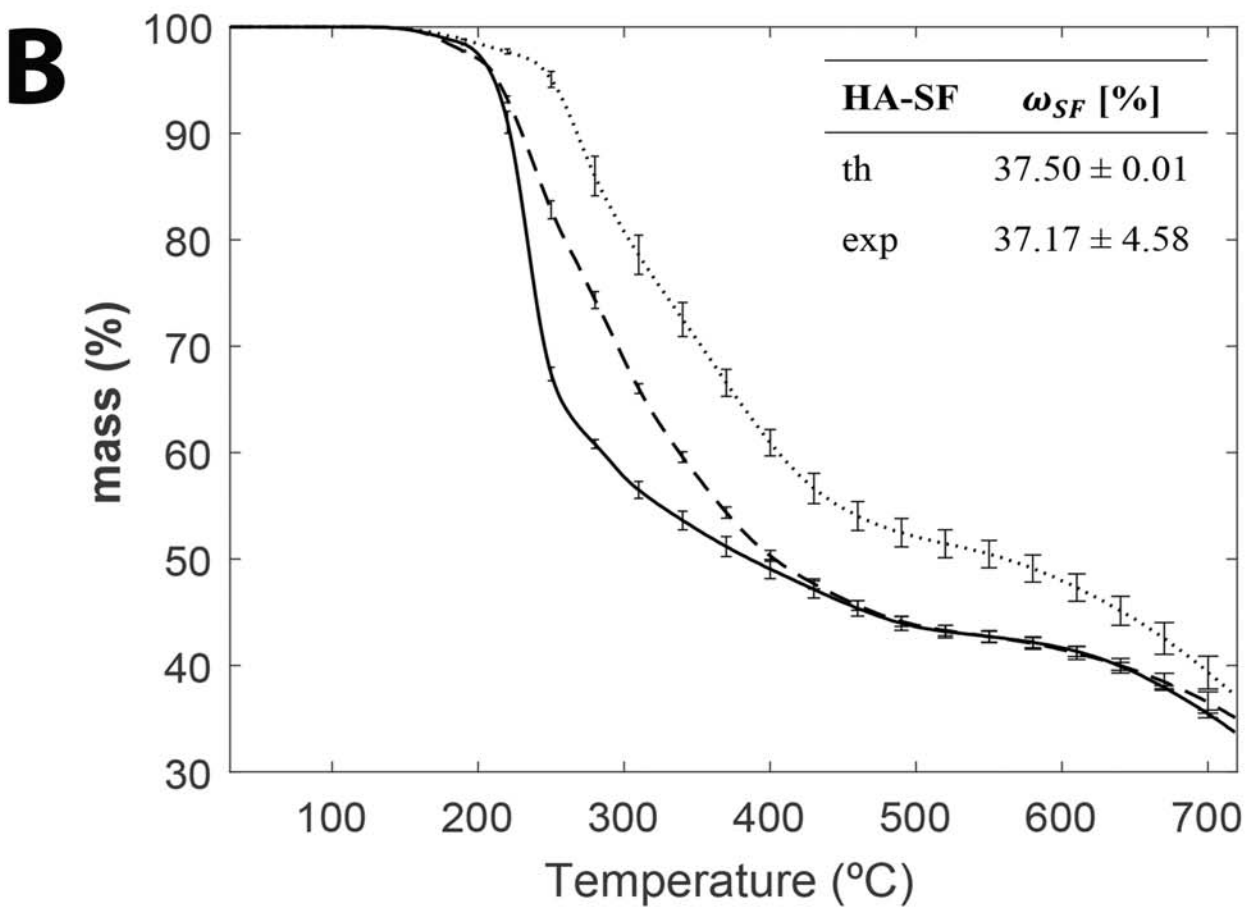
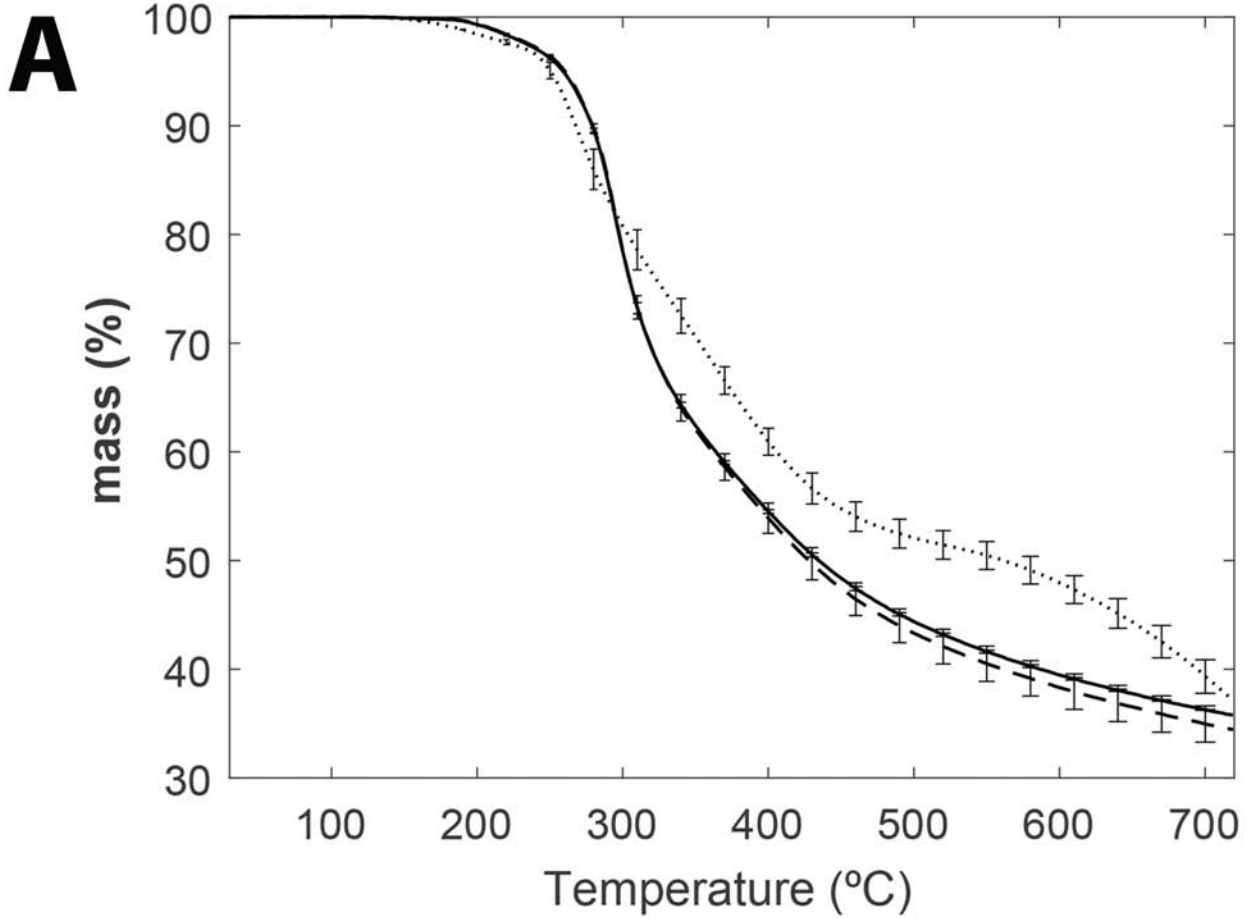
**Fig. 7.** HA and HA-SF scaffolds were implanted subcutaneously by means of two independent skin incision of approximately 1 cm on the back of each mouse. The skin sections containing the scaffolds were photographed at 1 (A and B for HA and HA-SF scaffolds, respectively), 4 (C and D for HA and HA-SF scaffolds, respectively) and 8 (E and F for HA and HA-SF scaffolds, respectively) weeks after their implantation. Healthy tissue can be observed surrounding the scaffolds since week 1. A high

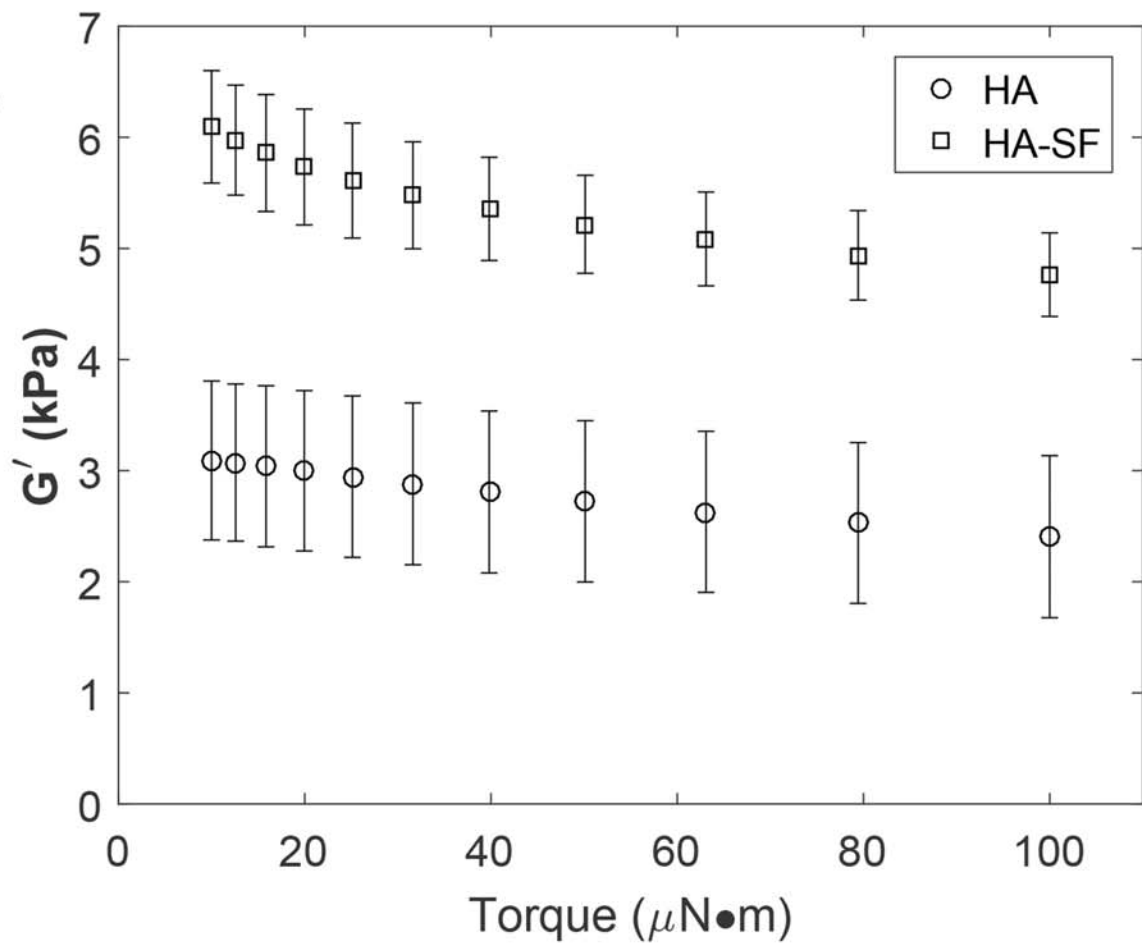
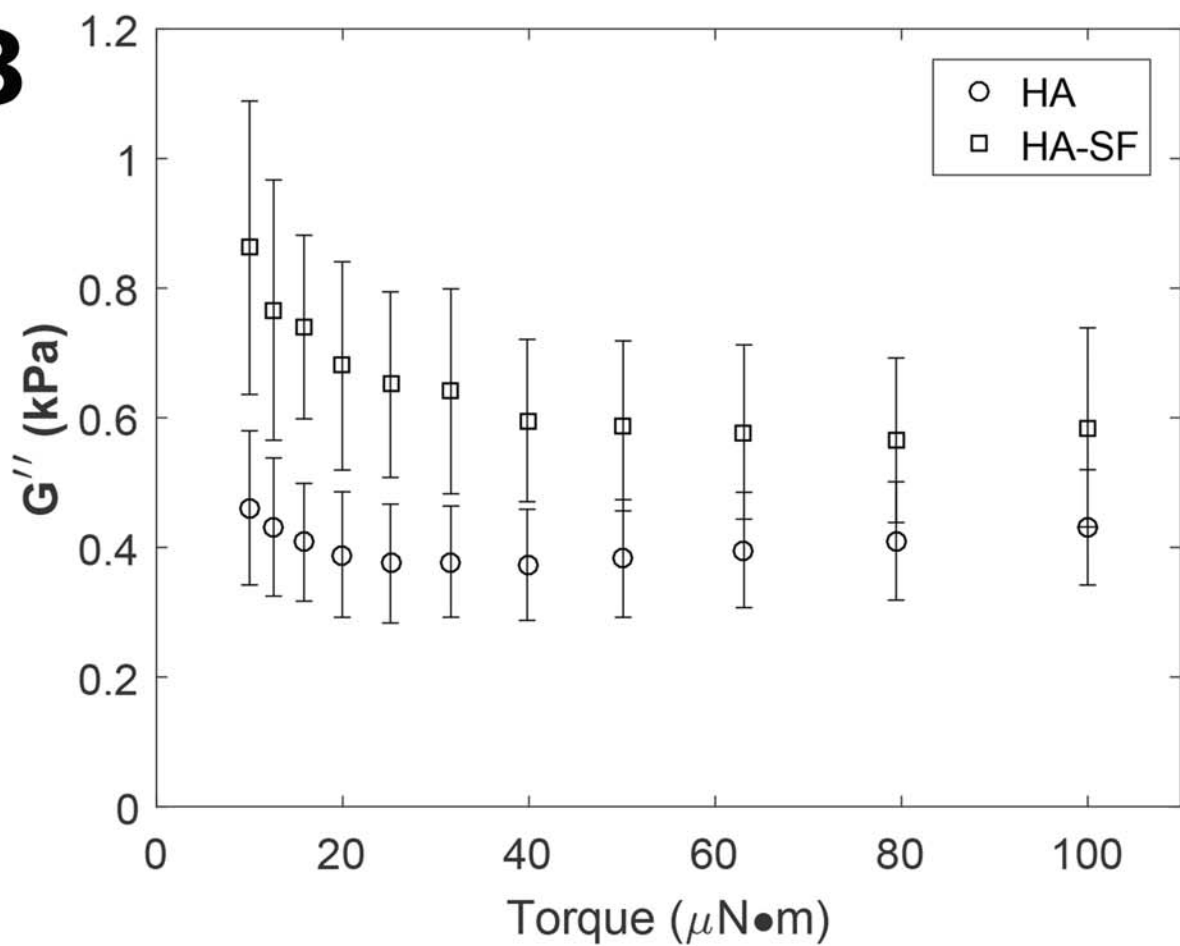
capillarity (white arrows) that is near to or in direct contact with the scaffolds is also visible since the first week. Scale bars = 2 mm.

**Fig. 8.** Cross sections of representative HA scaffolds stained with H&E and Masson's trichrome. One week after the implantation of the scaffold, an acute moderate foreign body reaction can be observed, with a large infiltration of granulocyte populations (A and B for H&E staining, C and D for Masson's trichrome staining). A fibrous capsule surrounding the scaffold is clearly visible which is a typical reaction after the implantation of a biomaterial. After 4 weeks, a reduction of the immune response can be observed, corresponding to a mild foreign body reaction (E and F for H&E staining, G and H for Masson's trichrome staining). The population of granulocytes has been reduced and there is a greater presence of macrophages. After 8 weeks, the scaffold has been completely resorbed and assimilated into the native tissue (I and J for H&E staining, K and L for Masson's trichrome staining). The fibrous capsule has disappeared and there are no granulocytes present. Now the cells present are mainly macrophages and active fibroblasts. Also, an increase of collagen structures inside the scaffold can be observed thanks to the fact that active fibroblasts have managed to invade the biomaterial. Many cross-sections of blood vessels are also visible after 8 weeks. Scale bar = 2 mm (A, C, E, G, I and K) and 500  $\mu\text{m}$  (B, D, F, H, J and L).

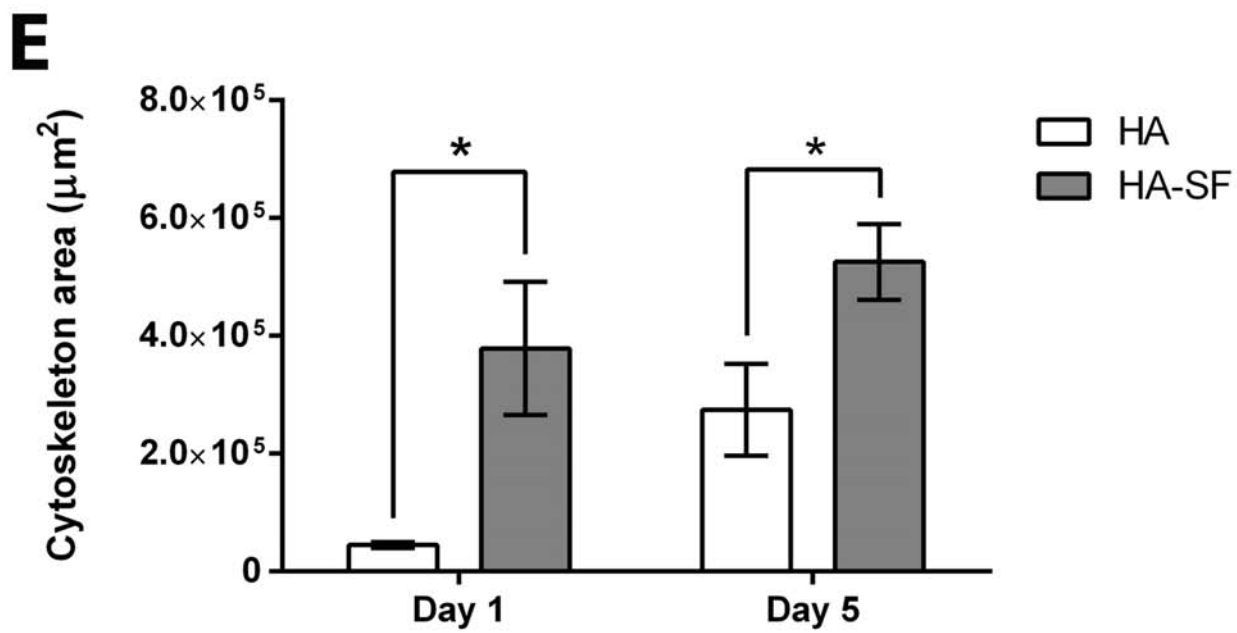
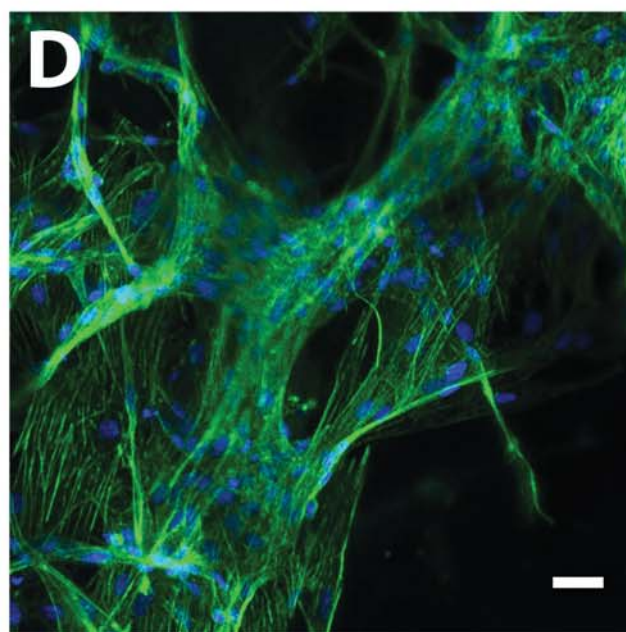
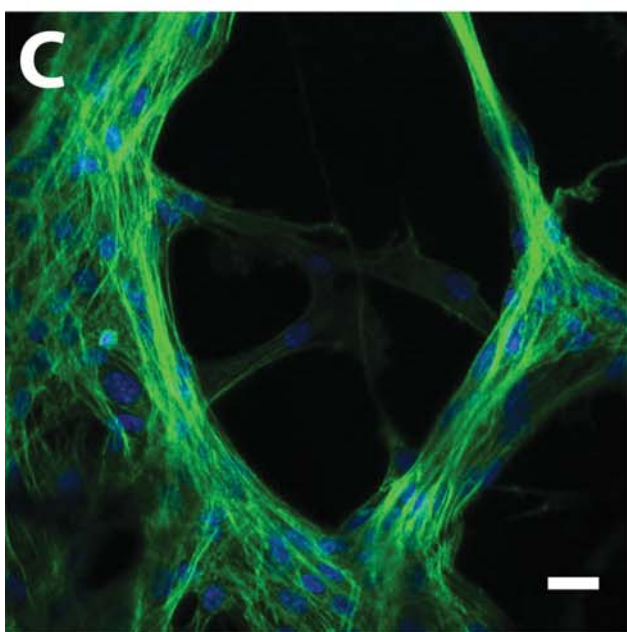
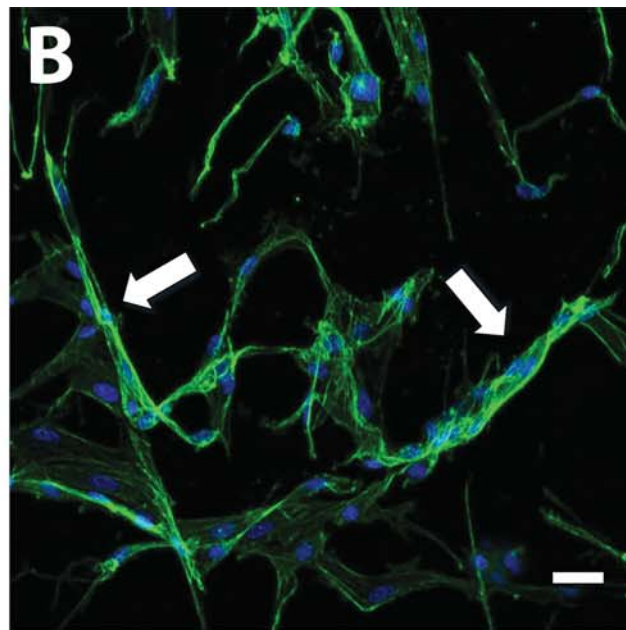
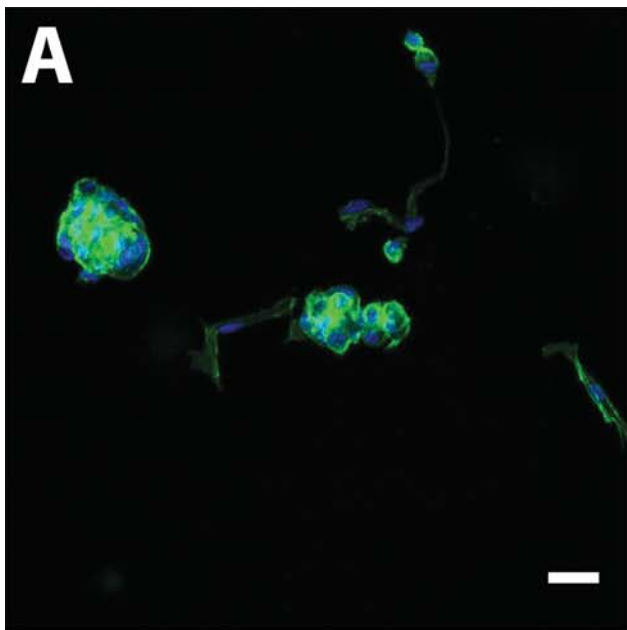
**Fig. 9.** Cross sections of representative HA-SF scaffolds stained with H&E and Masson's trichrome. One week after the implantation of the scaffold a fibrous capsule surrounding the scaffold is clearly visible, corresponding to an acute moderate foreign body reaction (A and B for H&E staining, C and D for Masson's trichrome staining). An infiltration of granulocyte populations is also observed. After 4 weeks, a clear reduction of the immune response can be observed, since there is a clear presence of blood vessels and collagen networks inside the scaffold and the population of granulocytes has been reduced (E and F for H&E staining, G and H for Masson's trichrome staining). After 8 weeks, the fibrous capsule has disappeared and there are no granulocytes present, so the scaffold has been completely resorbed and assimilated into the native tissue (I and J for H&E staining, K and L for Masson's trichrome staining). Now the cells present are mainly macrophages and active fibroblasts. Many collagen structures and cross-sections of blood vessels can be observed. Scale bar = 2 mm (A, C, E, G, I and K) and 500  $\mu\text{m}$  (B, D, F, H, J and L).

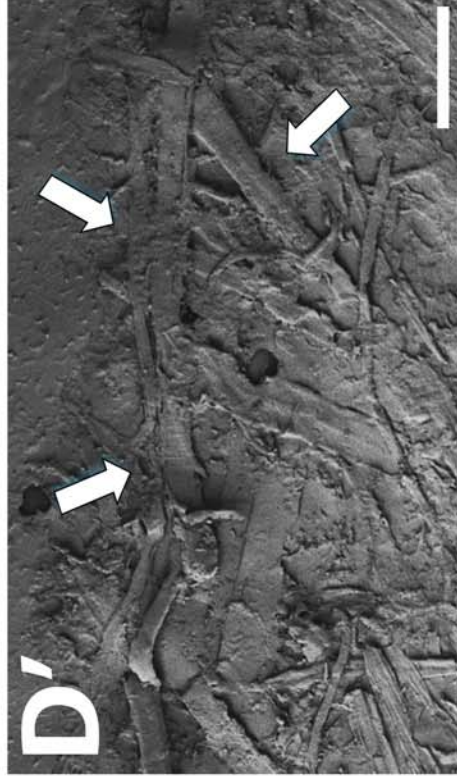
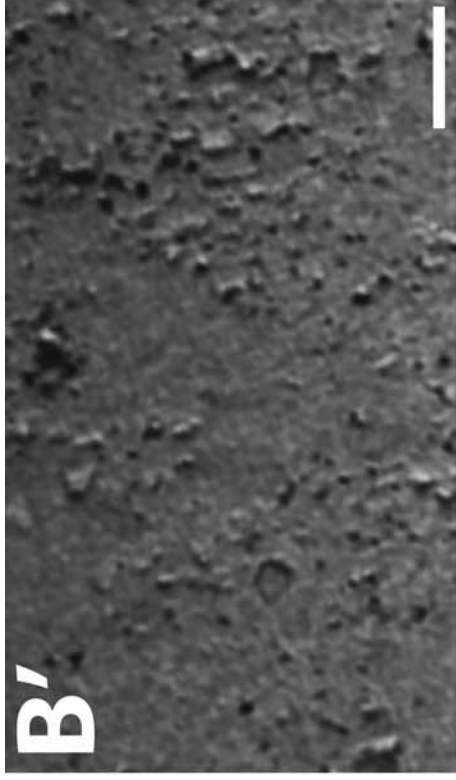
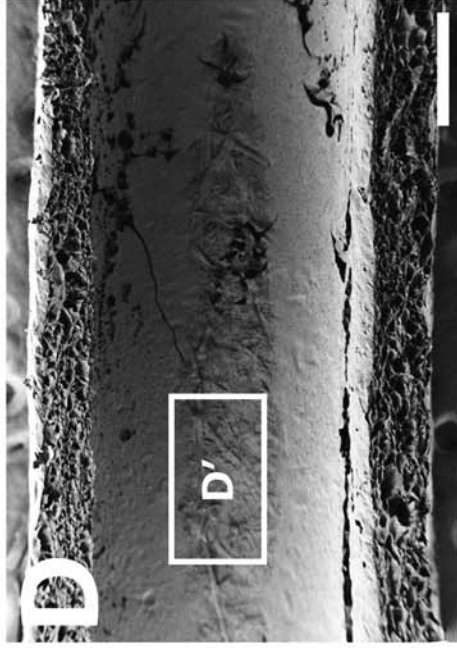
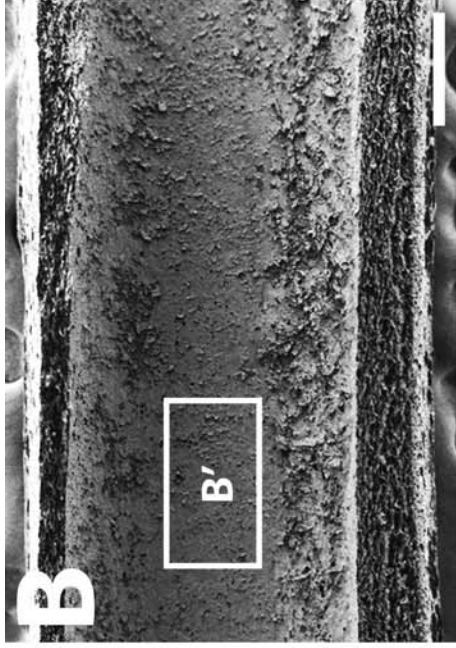
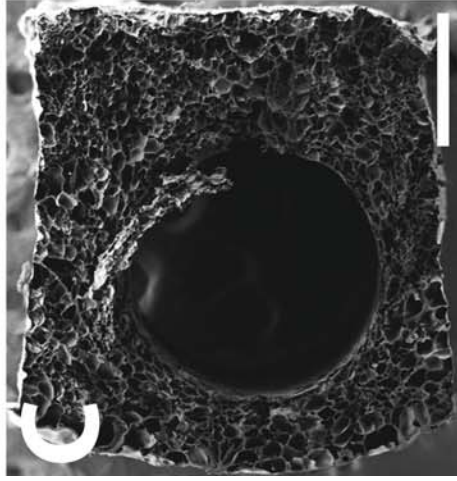
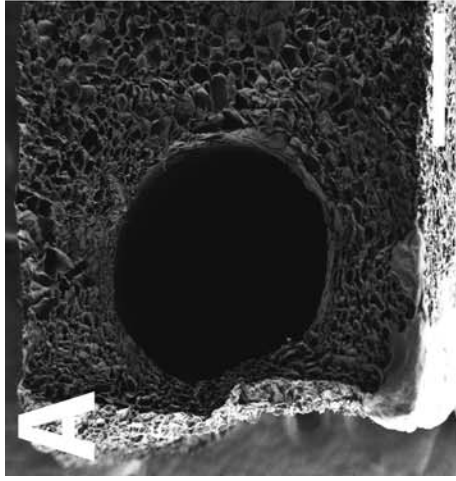
**Fig. 10.** Details of cross sections of representative HA and HA-SF scaffolds after 8 weeks of implantation. A and B: HA scaffold stained with Masson's trichrome. C and D: HA-SF scaffold stained with Masson's trichrome. In these images both the collagen deposition and the vascularization of HA and HA-SF scaffolds after 8 weeks of implantation are observable. Multiple collagen fibres (blue arrows) surrounded by active fibroblasts (green arrows) and cross-sections of blood vessels (red arrows) within the scaffold confirm the deposition of new extracellular matrix and the process of angiogenesis, respectively. The scaffold walls are indicated by black arrows. Scale bar = 200  $\mu\text{m}$  (A, C) and 100  $\mu\text{m}$  (B, D).

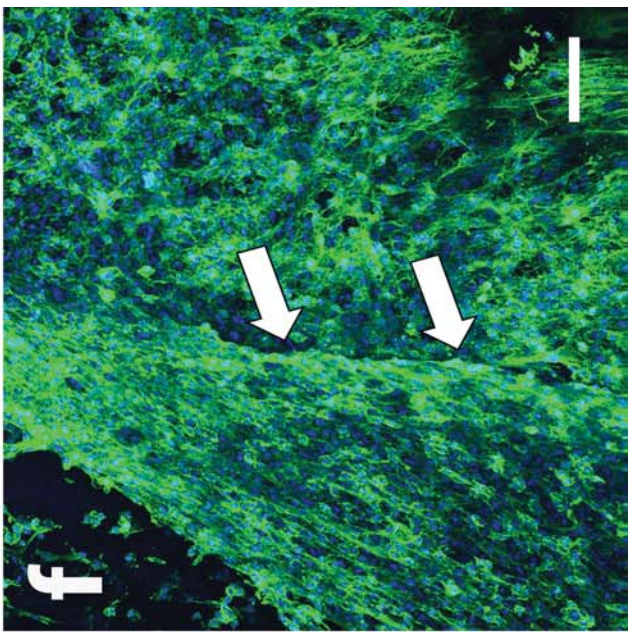
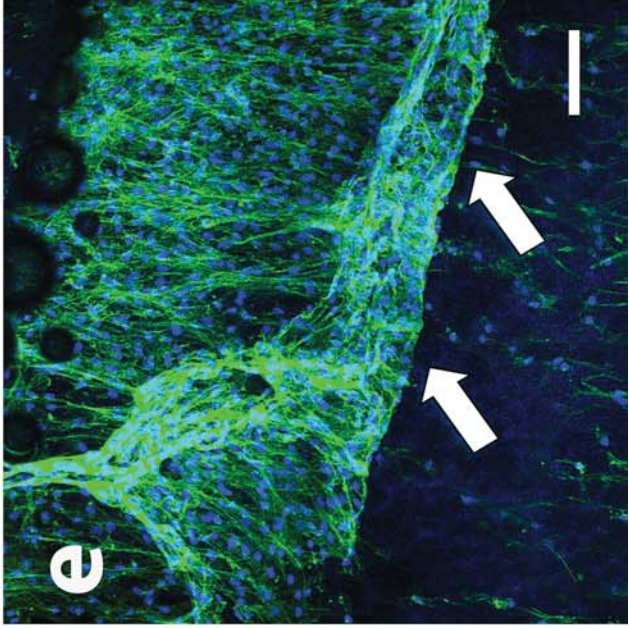
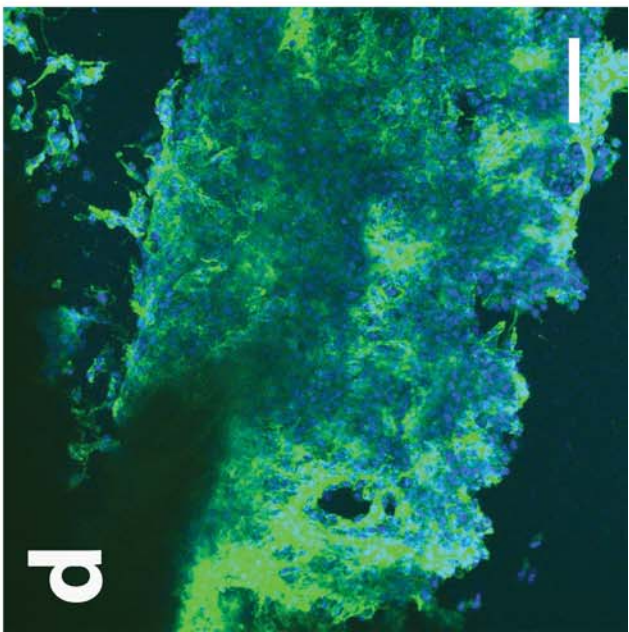
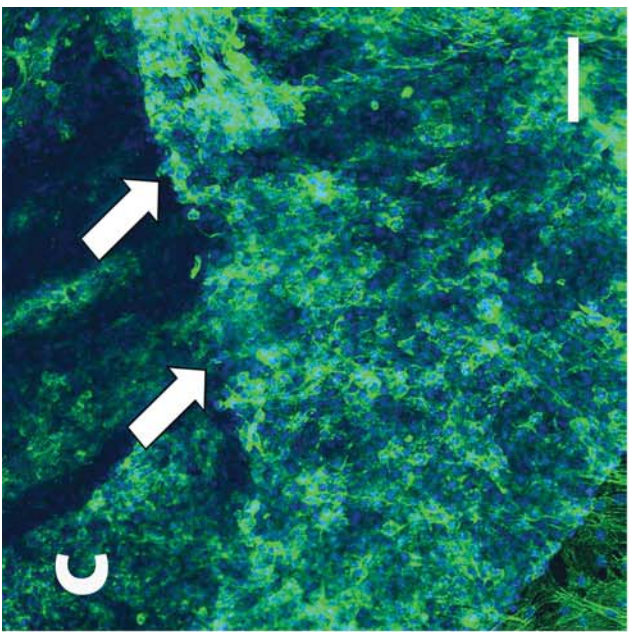
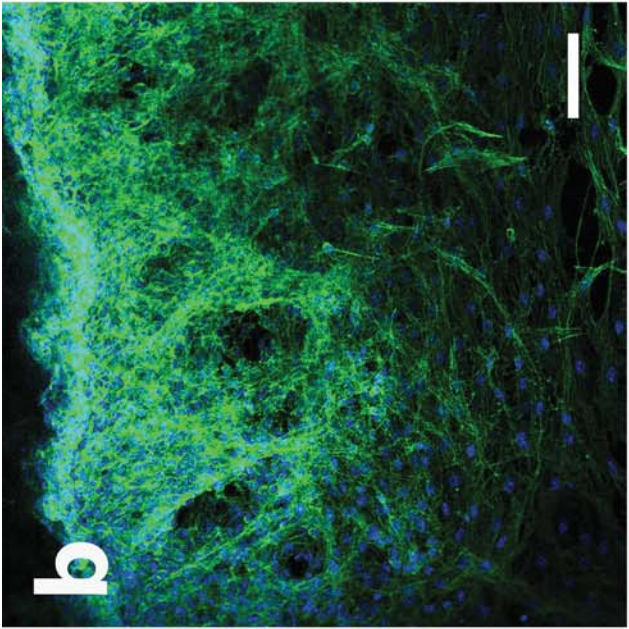
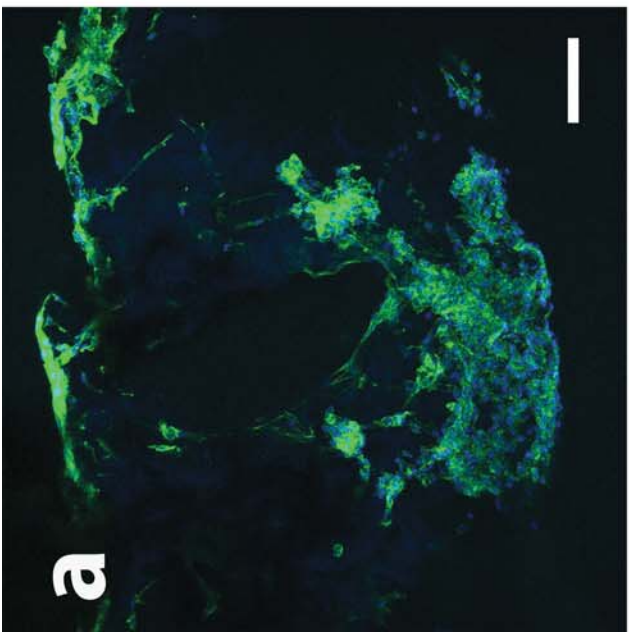


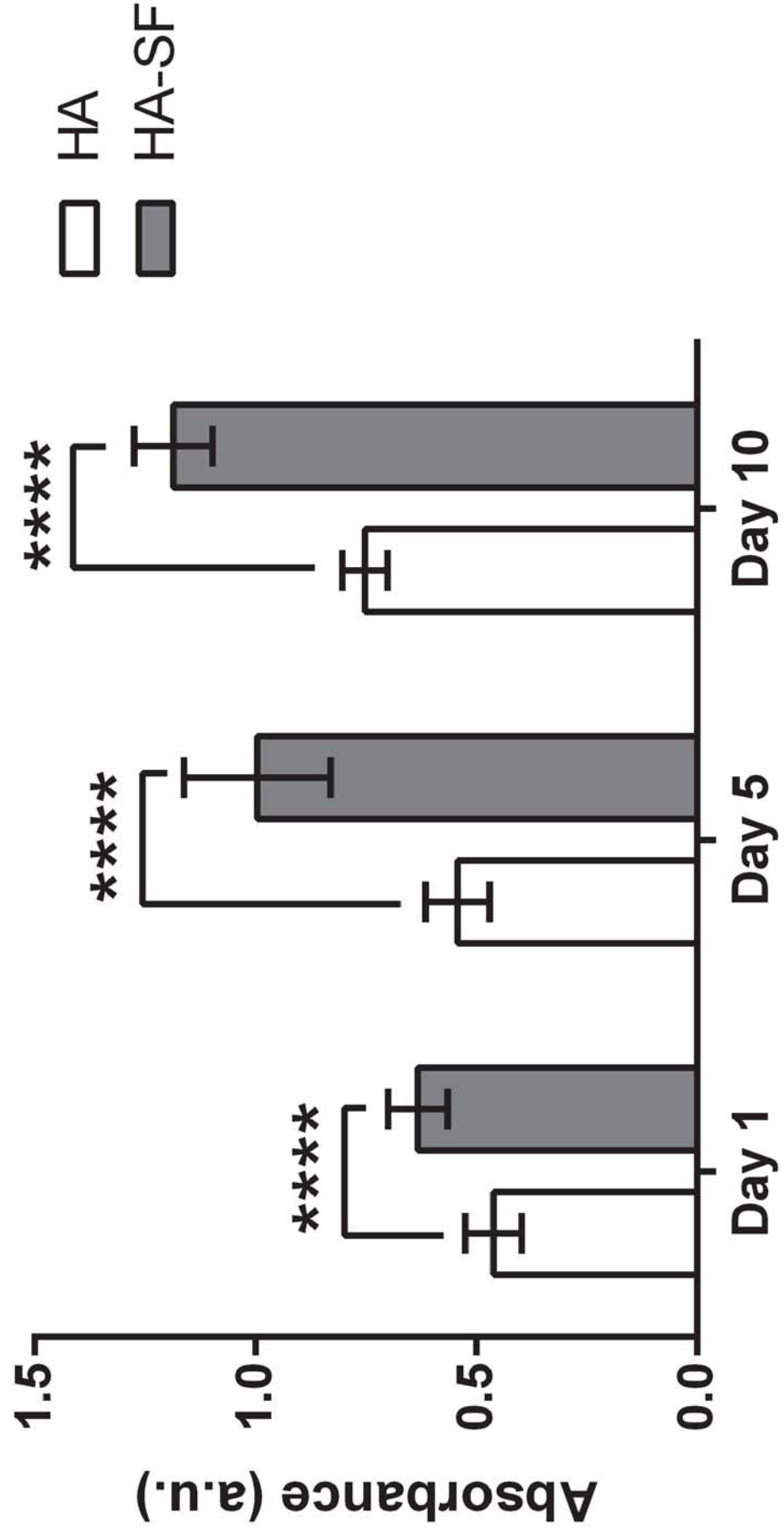
**A****B**

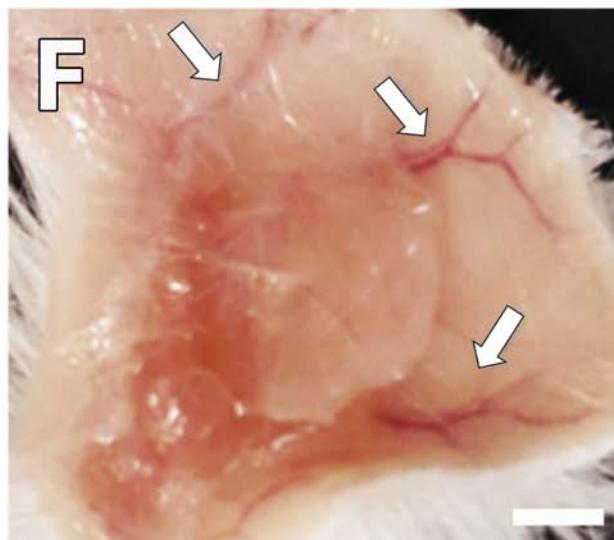
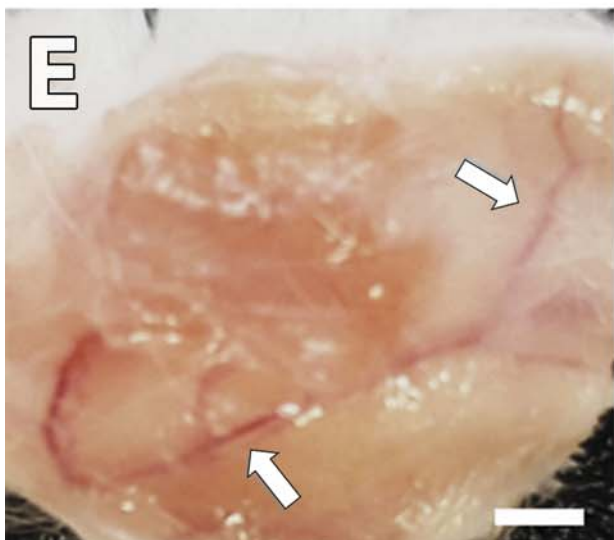
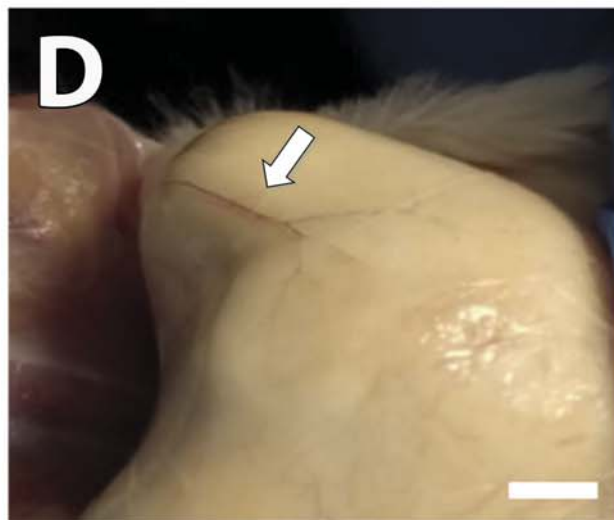
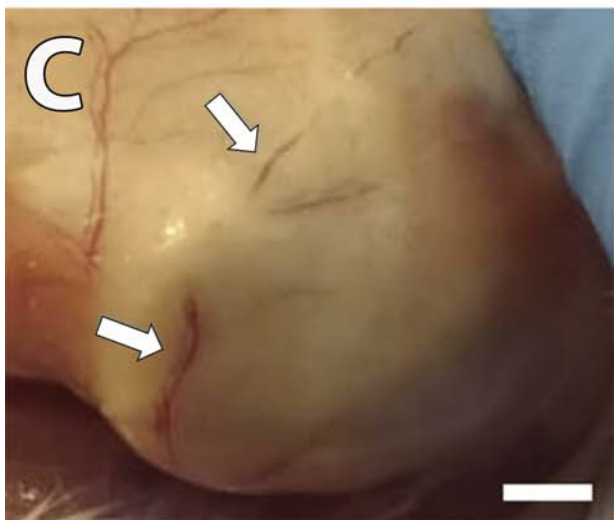
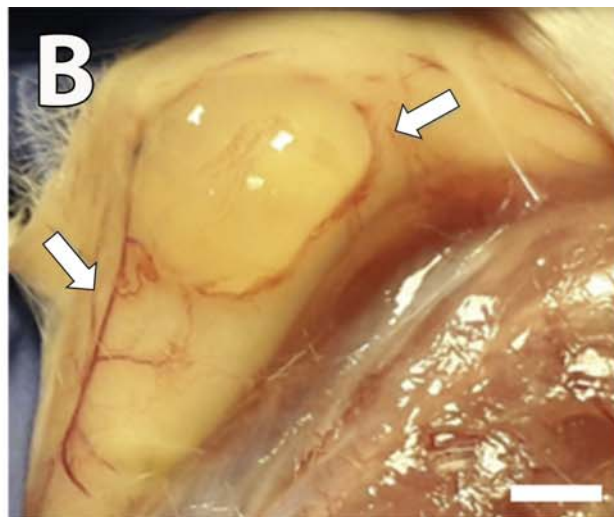
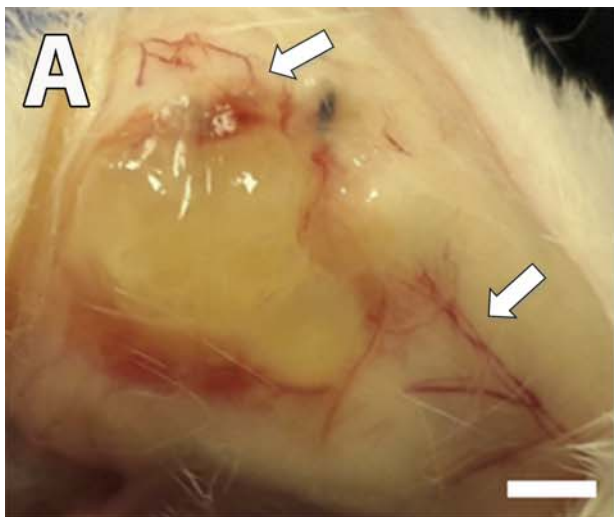


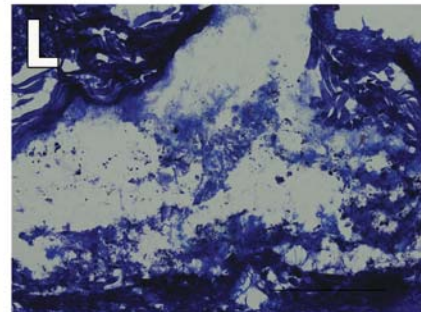
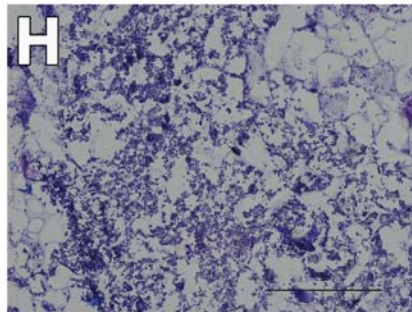
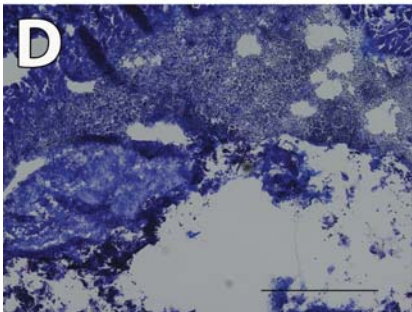
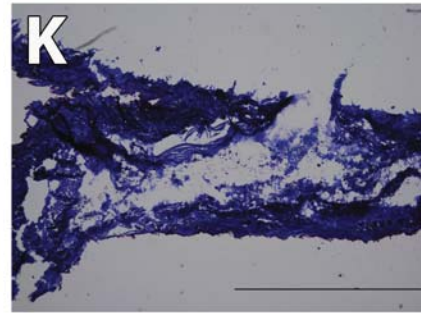
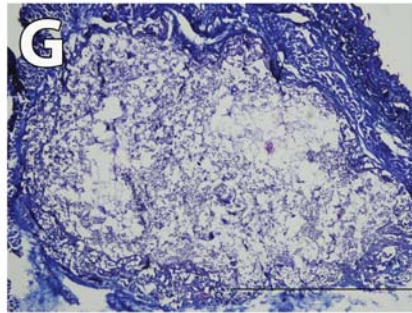
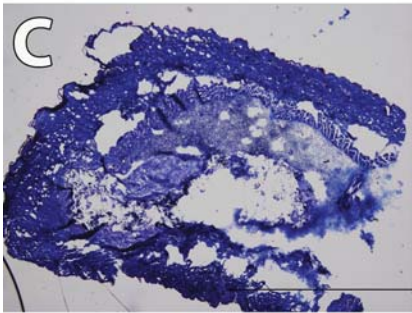
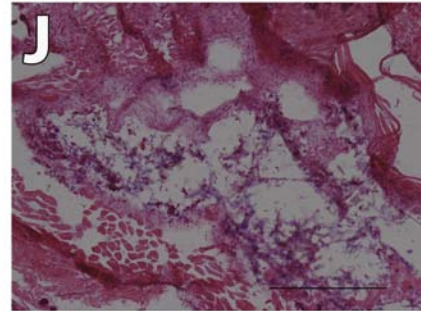
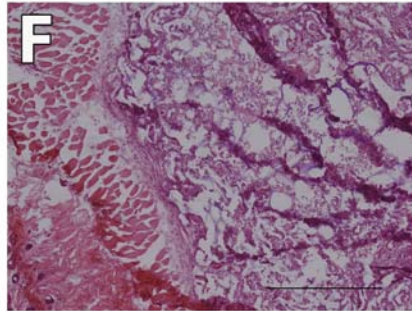
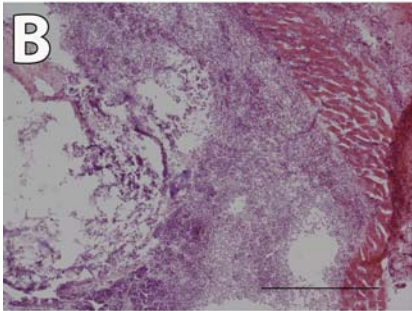
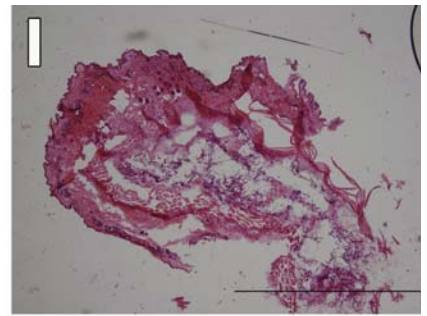
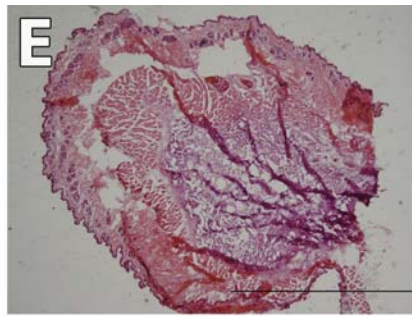
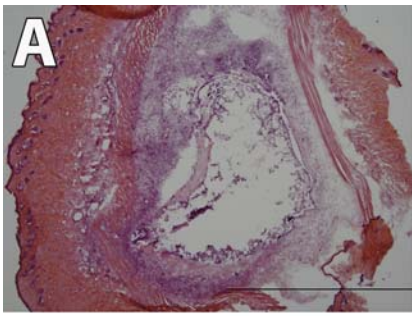


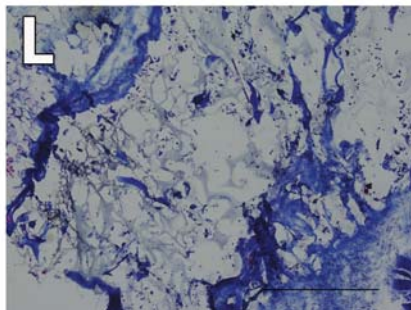
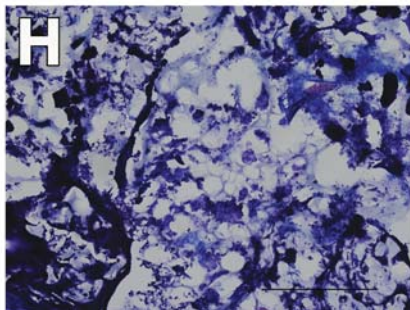
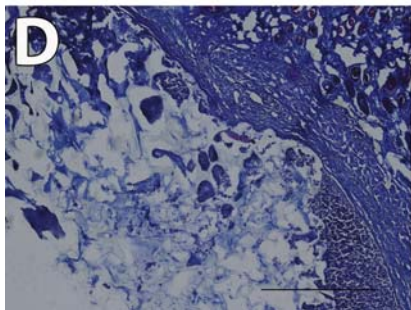
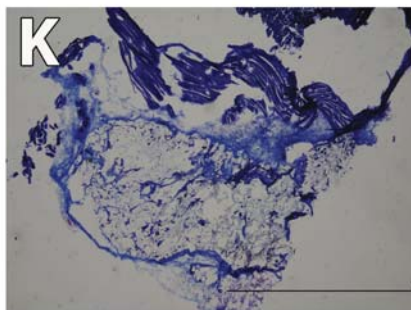
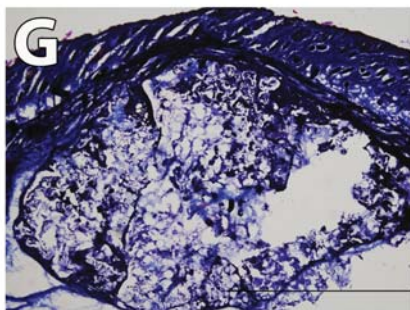
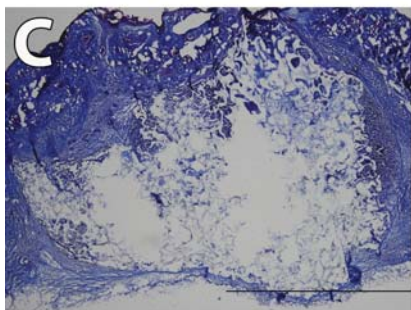
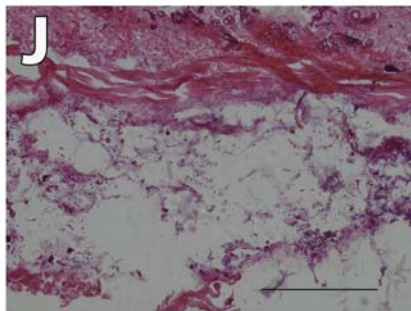
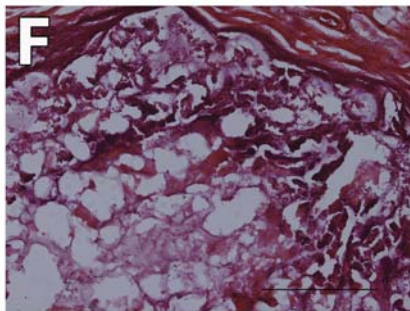
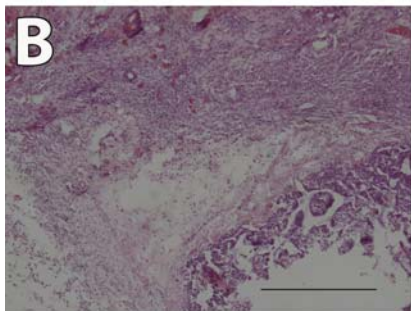
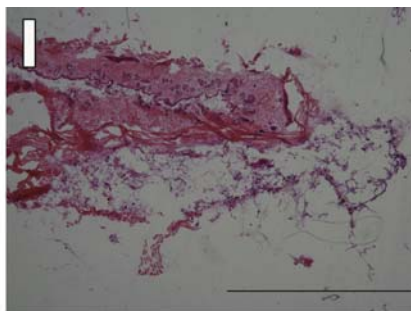
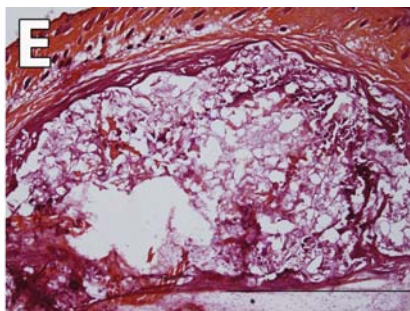
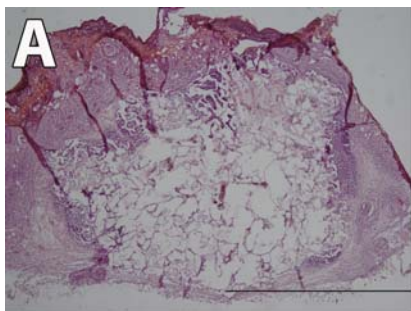


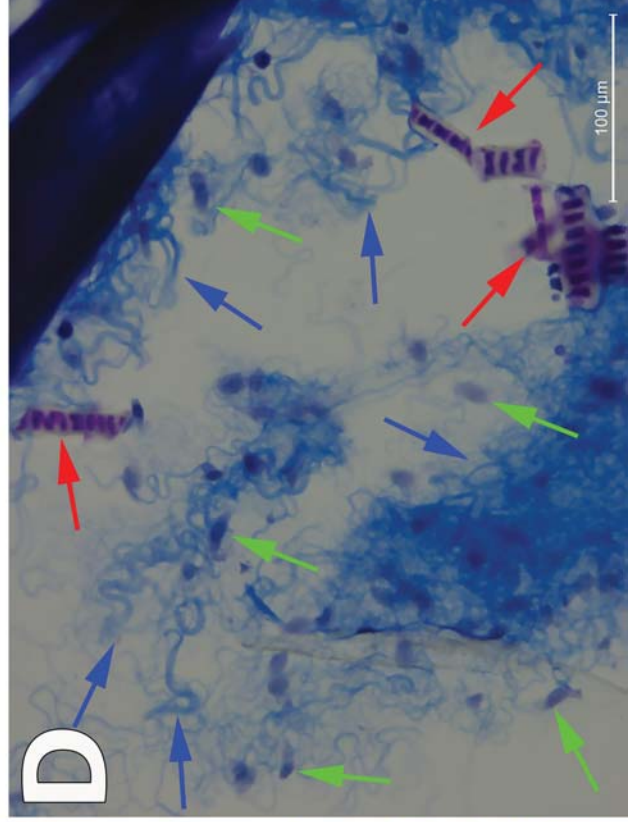
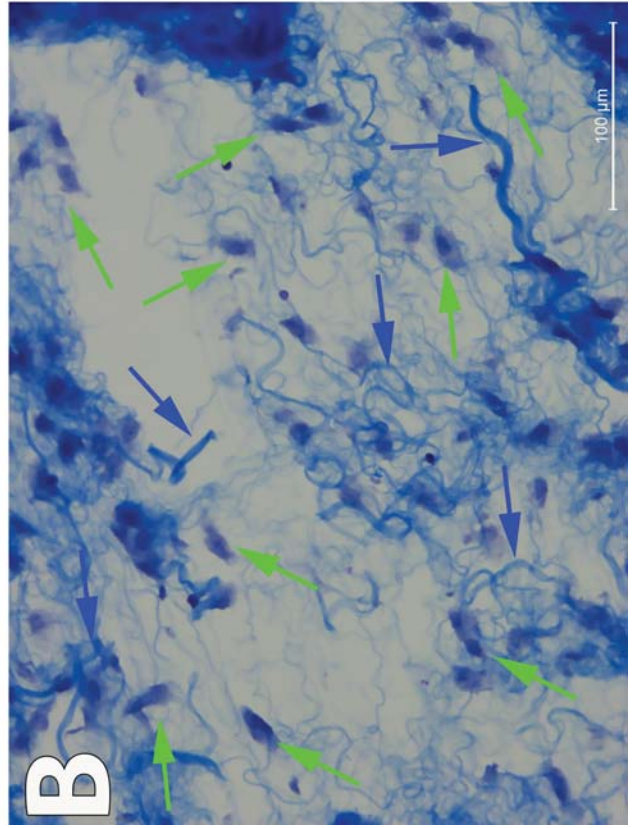
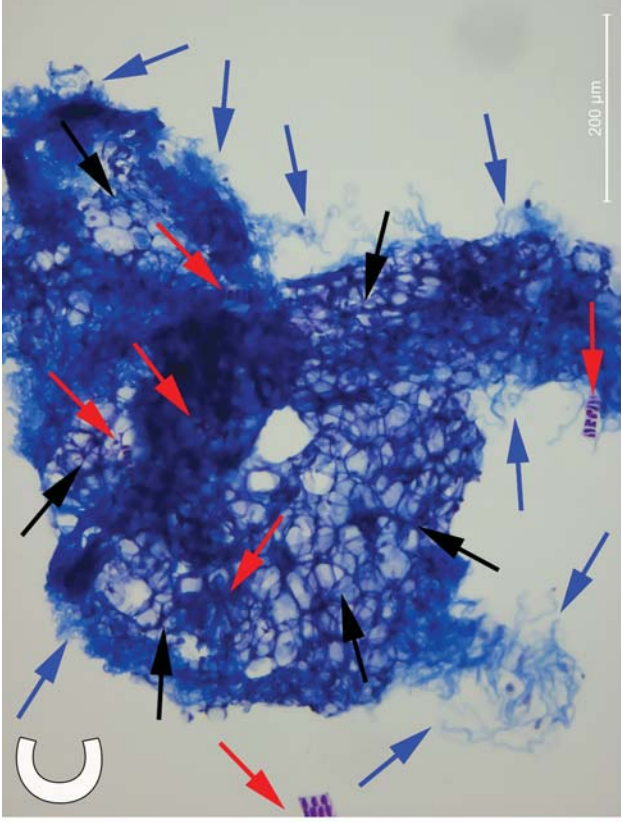
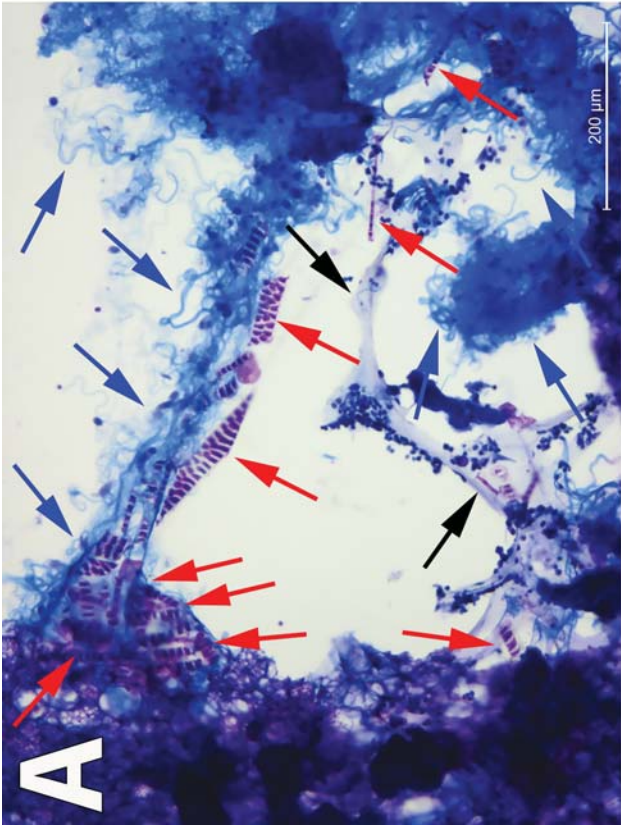














The corresponding authors confirm that all authors have seen and approved the manuscript to be considered for publication in *International Journal of Biological Macromolecules*.



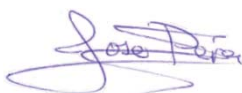
**Fernando Gisbert Roca**

*Center for Biomaterials and Tissue Engineering, Universitat Politècnica de València, Cno. de Vera s/n, 46022 Valencia, Spain*



**Paloma Lozano Picazo**

*CIBER-BBN, Biomedical Research Networking Center in Bioengineering Biomaterials and Nanomedicine, Spain. Centro de Tecnología Biomédica.*



**Jose Pérez Rigueiro**

*CIBER-BBN, Biomedical Research Networking Center in Bioengineering Biomaterials and Nanomedicine, Spain. Centro de Tecnología Biomédica. Universidad Politécnica de Madrid. Departamento de Ciencia de Materiales. ETSI Caminos, Canales y Puertos., Universidad Politécnica de Madrid.*



**Gustavo Victor Guinea**

*CIBER-BBN, Biomedical Research Networking Center in Bioengineering Biomaterials and Nanomedicine, Spain. Centro de Tecnología Biomédica. Universidad Politécnica de Madrid. Departamento de Ciencia de Materiales. ETSI Caminos, Canales y Puertos., Universidad Politécnica de Madrid.*



**Manuel Monleón Pradas**

*Center for Biomaterials and Tissue Engineering, Universitat Politècnica de València, Cno. de Vera s/n, 46022 Valencia, Spain*



**Cristina Martínez-Ramos**

*Center for Biomaterials and Tissue Engineering, Universitat Politècnica de València, Cno. de Vera s/n, 46022 Valencia, Spain*